CO_2 Capture by Aqueous Absorption
Summary of 3rd Quarter Progress Reports 2007

Supported by the Luminant Carbon Management Program
and the
Industrial Associates Program for CO_2 Capture by Aqueous Absorption

By Gary T. Rochelle
Department of Chemical Engineering
The University of Texas at Austin
November 19, 2007

1. Introduction

This research program is focused on the technical obstacles to the deployment of CO_2 capture and sequestration from flue gas by alkanolamine absorption/stripping and on integrating the design of the capture process with the aquifer storage/enhanced oil recovery process. The objective is to develop and demonstrate evolutionary improvements to monoethanolamine (MEA) absorption/stripping for CO_2 capture from coal-fired flue gas. The Luminant Carbon Management Program and the Industrial Associates Program for CO_2 Capture by Aqueous Absorption support 12 graduate students. Nine of these students have prepared detailed quarterly progress reports for the period July 1, 2007 to September 30, 2008. Some of these reports also include draft manuscripts, draft dissertations, and other written reports.

2. Conclusions

3.1 Ion chromatography analysis has identified eight oxidative degradation products in MEA and PZ: ammonia, ethylenediamine, formate, oxalate, nitrite, nitrate, formate and glycolate.
3.2 AMP is resistant to oxidative degradation
4.1 Piperazine has been shown to have little, if any thermal degradation by cation chromatography, HPLC, pH titration, and NMR analysis at standard stripper conditions, 120°C - 135°C, over an 8 week time span.
4.2 11m MEA solution with a loading of 0.5 mol CO_2/mol amine exhibits a loss of more than 60 wt% MEA at 135°C after 8 weeks.
5.1 At 40°C in 4 M MDEA/1.2 M PZ the volatility of PZ varies from 18 to 4 ppm as the loading increases to 1 mole CO_2/mole PZ. The MDEA volatility is about 6 ppm over the same range of conditions.
6.1 The effective wetted area of Mellapak 250Y did not vary with surface tension from 35 to 72 mN/m.
6.2 The effectve wetted area of Flexipak 1Y appears to be independent of viscosity from 0.8 to 5.5 mPa-s.
7.1 Intercooling is effective at L/G values that produce a temperature bulge in the middle of the column.

8.1 A RateSep stripping model of 4 m K/4 m PZ has demonstrated that the double matrix stripper requires an equivalent work of 39.7 kJ/mole CO_2 to get 10 MPa, compared to 42.0 kJ/mole for the simple stripper.
9.1 At 40^{o}C, 7 m MEA has a MEA vapor pressure of 0.008 kPa.
10.1 The ORP (oxidation-reduction potential) of loaded amine solution responds in less than 5 minutes to changes in agitation and aeration in experiments of oxidative degradation.

3. Oxidative Degradation of Amines – Andrew Sexton

Aqueous monoethanolamine (MEA) and piperazine (PZ) solutions were batch loaded into glass jacketed reactors and subjected to oxidative degradation via a high gas flow and low gas flow degradation apparatus. Amine solutions were degraded in the low gas flow apparatus using 100 mL/min of a 98% O_2/2% CO_2 saturated gas mixture in which mass transfer was achieved by vortexing. Liquid samples were withdrawn from the reactor during the course of the experiment and analyzed for degradation using ion chromatography. The high gas flow degradation apparatus employed 7.5 L/min of an air/2% CO_2 mixture diluted with N_2 to achieve 15% O_2; oxygen mass transfer in this apparatus takes place by sparging the saturated gas mixture through the solution and by vortexing. A Fourier Transform Infrared Analyzer collects continuous gas-phase data on amine volatility and volatile degradation products.

Ion chromatography analysis has been used to identify and quantify eight oxidative degradation products in MEA and PZ systems: ammonium, ethylenediamine, formate, oxalate, nitrite, nitrate, formate and glycolate.

Formate is the most abundant degradation product observed in 7 molal MEA systems, followed by nitrate/nitrite, then oxalate. Iron and copper-catalyzed systems produce similar amounts of formate; a combination of both catalysts enhances the production of formate. Iron-catalyzed systems produce twice the amount of nitrite/nitrate as do Cu systems. Degradation inhibitor "A" reduced the formation of observable oxidative degradation products by 70%.

Aqueous piperazine systems were degraded in the presence of iron, copper and/or vanadium catalysts. Aqueous piperazine systems behaved differently to 7 m MEA systems in the presence of copper and iron; degraded MEA systems favored the formation of carbon-containing degradation products, while PZ favored nitrogen-containing products. The addition of 100mM inhibitor "A" resulted in a 91% to 93% reduction in the concentration of oxidative degradation products for Fe/Cu systems, and a 70% reduction for vanadium-catalyzed systems. The addition of 5 molal potassium ion to an aqueous piperazine solution effectively inhibits any oxidative degradation in PZ systems. K^+ ion significantly reduces O_2 solubility in PZ systems.

Formate was produced at a rate of 2.35 mM/hr in a 7m MEA/2m PZ system catalyzed by iron and copper, which was the highest rate observed for any of the degradation experiments. The addition of 100 mM inhibitor "A" reduced degradation rates by 81%. Even with this reduction in product formation, combined MEA/PZ systems are a less attractive option than MEA or PZ-only systems in terms of oxidative degradation. Moreover, preliminary IC analysis shows 2-amino-1-methyl-1-propanol (AMP, a sterically hindered amine) systems to be more degradation resistant than inhibited MEA and PZ systems by approximately 85%.

The body of this report is included in full text of the Department of Energy final report.

4. Thermal Degradation - Jason Davis

Piperazine has been shown to have little, if any thermal degradation by cation chromatography, HPLC, pH titration, and NMR analysis at standard stripper conditions, 120°C - 135°C, over an 8 week time span. As a comparison, an 11m MEA solution with a loading of 0.5 mol CO_2/mol amine exhibits a loss of more than 60 wt% MEA at 135°C after 8 weeks.

5. Thermodynamics of MDEA/PZ/CO_2/H_2O - Bich-Thu Nguyen

This work explores the volatility of MDEA and PZ in blends of varying amine concentrations at 40ºC and 60ºC. Amine volatilities are reported in terms of partial pressures and are further analyzed in terms of their apparent activity coefficients as a function of loading, temperature, and amine concentration. PZ partial pressure is found to decrease steadily as CO_2 loading, reported on a basis of mol CO_2/mol PZ, is increased. Furthermore, as expected this partial pressure is higher with respect to the higher experimental temperature and concentration. As for the apparent PZ activity coefficient, it behaves the same as the partial pressure with respect to all the experimental variables mentioned. Conversely, the apparent MDEA activity coefficient is seen to be higher with respect to the lower experimental temperature (40ºC) and also with lower MDEA concentrations.

6. Influence of Liquid Properties on Effective Mass Transfer Area of Structured Packing - Robert Tsai

(Also supported by the Separations Research Program}

The effective mass transfer area of Sulzer Mellapak 250Y structured packing has been measured via CO_2 absorption into dilute caustic solution at high (72 mN/m) and low (35 mN/m) surface tension. The results were practically identical, implying that the liquid spreadability on the packing surface was equivalent in both cases. Sessile drop contact angle data were obtained in an effort to understand and justify the observed phenomenon. Initial measurements on a textured Mellapak surface were unsuccessful, so an un-textured (smooth) stainless steel sheet was tested instead. The high and low surface tension fluids had noticeably different contact angles (70˚ vs. 40˚) on this surface. It is suspected that the observed spreading behavior was primarily dictated by the properties of the packing and not those of the liquids.

The effective mass transfer area of Koch-Glitsch Flexipac 1Y structured packing was evaluated as a function of liquid load with a viscosity-enhanced caustic solution ($\mu \sim$ 5.5 mPa·s, $\sigma \sim$ 57 mN/m). A comparison with the baseline data ($\mu \sim$ 0.8 mPa·s, $\sigma \sim$ 72 mN/m) showed that the physical property modifications had no tangible effect.

7. Modeling of CO_2 Absorption by Aqueous Amines: Intercooling – Jorge Plaza

Intercooling has been proposed as an alternative to increase absorber performance in the capture of CO_2. Analysis has been done on 11 *m* MEA and 4.5 *m* K_2CO_3/4.5 *m*

piperazine absorbers using a double matrix stripper. In this quarter the effect of loading in the lean feed was evaluated for a simple absorber using the latter solvent. Complete analysis of the effect of intercooling at different loading conditions allowed the determination of an optimum bracket for the implementation of this alternative. This optimum is related to the position of the temperature bulge within the absorber. All of the results from the intercooling analysis were gathered and a first article draft has been written and is attached to this report. Future work will focus on the development of an MEA absorber model.

8. Modeling Stripper Performance for CO_2 Removal – David Van Wagener

A model was developed in Aspen Plus® which collated the entire absorption/stripping process for CO_2 removal using 4 m K^+/4 m PZ into one simulation, and it was optimized to require a minimum equivalent work. The double matrix stripper configuration was used for the stripping section, and the simulation was also compared to a simple stripper baseline. Removal of CO_2 and subsequent compression to 10 MPa required 39.7 kJ/mol CO_2 and 42.0 kJ/mol CO_2 for the double matrix and simple stripper arrangements, respectively. Previous research projected that the savings using a double matrix stripper would be 5.8 kJ/mol CO_2, more than double what this work suggests. This difference is attributed to the non-optimal lean loading used in previous research, which increases the difference between double matrix and simple stripper performance due to the system's high sensitivity to lean loading. This quarter's work also determined that the previously used five degree hot side approach for the heat exchangers is infeasible because a temperature crossover exists. A five degree cold side approach must be used, which corresponds to a ten degree hot side approach for this case.

9. Thermodynamic Modeling – Marcus Hilliard

Six chapters are attached from the dissertation of Marcus Hilliard. This work includes regressions for the 6 systems: pure MEA and PZ, MEA/H_2O, PZ/MEA/H_2O, MEA/N_2O/H_2O, and K_2CO_3/CO_2/H_2O. The defense of the dissertation is scheduled for January 14, 2008.

The vapor pressure data for pure components was regressed as a function of temperature to obtain consistent values of the liquid heat capacity of piperazine and MEA. At 40^{o}C, 7 m MEA has a MEA vapor pressure of 0.008 kPa. The heat capacity of protonated MEA was adjusted to provide a consistent representation of the temperature dependence of the pK_a of MEA. The measured amine vapor pressures of MEA and PZ over unloaded blends of MEA/PZ were modeled with the parameters from the single amine/water systems. The physical solubility of CO_2 in MEA was modeled from the data on the solubility of N_2O The model of the K_2CO_3/CO_2/H_2O incorporates data on CO_2 solubility, activity of water. It is used to predict the solubility of solids in the solvent.

The body of this report is included in full text of the Department of Energy final report.

10. Oxidative Degradation at Stripper Conditions: Oxidation-Reduction Potential - Fred Closman

The research group has performed basic oxidation-reduction potential (ORP) experiments in order to assess the viability of using commercially available off-the-shelf ORP measurement equipment. We have measured ORP in ROC20 solutions under aerated and agitated conditions as well as quiescent conditions in a jacketed glass reactor maintained at 53.5°C. Our work has determined that the ORP of aerated systems varies with the amount of agitation and aeration in the system. In the presence of metals species (Cu^{2+}), ORP of solution immediately increased, while viscosity increased after three weeks of sitting idle. Practical findings included: (1) the presence of metals species in ROC20 at 0.01 mmolar increased the ORP of solution, and (2) commercially available ORP measurement equipment for the water industry can be adapted for amine solvent studies in the laboratory. Increases in viscosity to over 300 cP in a ROC20 solution may be evidence of polymerization of solvent after sitting idle, but no evidence of dimerization was found through basic cation exchange chromatography.

11. Reclaiming by Crystallization of Potassium Sulfate – Qing Xu

One side reaction in CO_2 capture when using MEA/PZ is the generation of sulfate from SO_2. This sulfate has to be removed so that the MEA/PZ solution can be reused for CO_2 capture. Potassium compounds can be used in the removal of sulfate. In order to determine how best to accomplish this, the solubility of potassium sulfate was measured with variable MEA/PZ concentration and CO_2 loading.

In previous work by Xu, solubility measurement was conducted at low temperatures up to 40ºC. A model predicting experimental K_{sp} was developed, with equivalent alkali concentration, temperature, and ionic strength as the variables.

In this report a new method was developed for conducting solubility measurement at high temperatures and high CO_2 loading. The experiment system was well sealed to avoid CO_2 loss under those conditions and got good data. Based on the previous work of Freguia (2002), new interaction parameters were regressed in this work to match Söhnel's data (1985) in water and the experiment data by Xu. The regression was done using Data Regression System in Aspen Plus®. An interaction parameter set for CO_2-MEA-H_2O-K^+-$SO_4^=$ system in Electrolyte-NRTL model was developed. The model is tested by a series of flash simulations. It can fairly simulate the interactions between ion pairs and molecules within certain condition ranges, but still needs further modification.

12. Dynamic Modeling of CO2 Stripping - Sepideh Ziaii Fashami

An accurate dynamic model for a process has to be both rigorous enough to reflect the process complexity and simple enough to ensure the feasibility of process simulations. For simulation of dynamic behavior of the stripper, fundamental understanding of mass and heat transfer in the presence of reactions is required. In addition, the simulator should use proper correlations that predict physical properties and parameters of reactions accurately. Therefore, we have developed correlations for predicting density and viscosity of loaded MEA solution based on available experimental data. We obtained concentration-based equilibrium constants, vapor pressure, heat of

absorption, and Henry's Law constant of CO_2 versus temperature, loading, and MEA concentration with E-NRTL framework modified by Hilliard (2007). In addition, the mass transfer mechanism in the presence of equilibrium reactions in the liquid phase is described and formulated.

Thermal Degradation
Progress Report, Q3, 2007

by Jason Davis

Luminant Carbon Management Program

Department of Chemical Engineering

The University of Texas at Austin

Abstract

Piperazine has been shown to have little, if any thermal degradation by cation chromatography, HPLC, pH titration, and NMR analysis at standard stripper conditions, 120°C - 135°C, over an 8 week time span. As a comparison, an 11m MEA solution with a loading of 0.5 mol CO_2/mol amine exhibits a loss of more than 60 wt% MEA at 135°C after 8 weeks.

Introduction

This subtask will be used to identify and measure thermal degradation of piperazine and piperazine blend solutions under potential absorber/stripper conditions. Piperazine (PZ) is a cyclic diamine that is being evaluated as an alternative to MEA. Currently, there is no literature on thermal degradation of PZ, but this subtask will be used to define possible degradation mechanisms and to show the rate of piperazine degradation, if any, under stripper conditions.

Theory

Monoethanolamine

Traditional thermal degradation in amine systems is characterized by a carbamate polymerization reaction. The first defined system was for monoethanolamine, MEA. Polderman, Dillon and Steele[1] describe the mechanism for thermal degradation of MEA by carbamate polymerization. In CO_2 capture, MEA associates with CO_2 in the absorber to form MEA carbamate as illustrated below.

This reaction is normally reversed in the stripper, but in some cases the MEA carbamate will cyclize to form 2-oxazolidone, which is also a reversible reaction, as shown below.

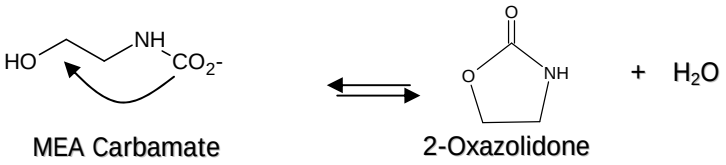

MEA carbamate can also irreversibly dehydrolize to form N,N'-di(2-hydroxyethyl)urea[2].

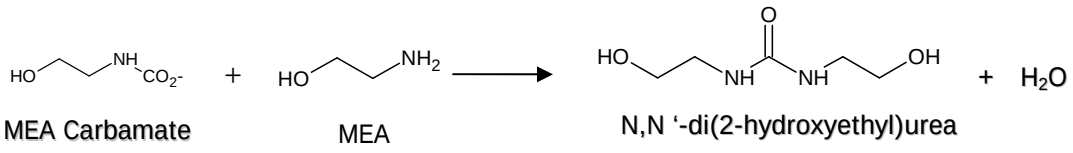

The former product, 2-Oxazolidone, can then react with another molecule of MEA to form 1-(2-hydroxyethyl)-2-imidazolidone which is sometimes referred to as HEIA.

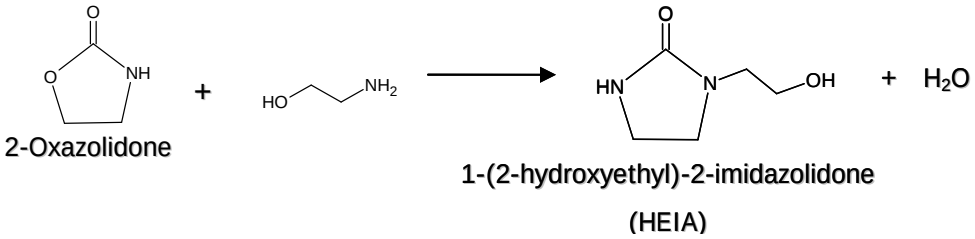

HEIA can then be hydrolyzed to form N-(2-hydroxyethyl)-ethylenediamine or HEEDA.

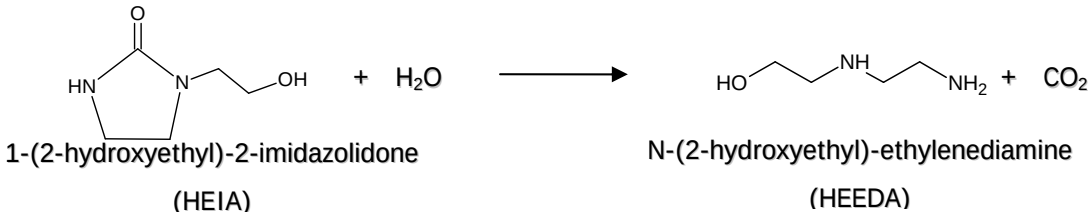

These four species (2-oxazolidone, dihydroxyethylurea, HEIA and HEEDA) plus further polymerization products are believed to be the main products of thermal degradation. The rate of formation of these products is a function of temperature (faster kinetics), CO_2 loading (more carbamate present) and MEA concentration.

Piperazine

The structure of piperazine (PZ) is a cyclic diamine that is shown below.

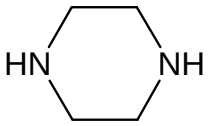

Piperazine

Since PZ does not have an alcohol group present like MEA, thermal degradation by the pathway shown for MEA above should be minimized since the initial reaction step will be eliminated. Other reaction pathways could exist like the one listed below in which the carbamate of one piperazine and the protonated amine of another piperazine molecule react to form a urea.

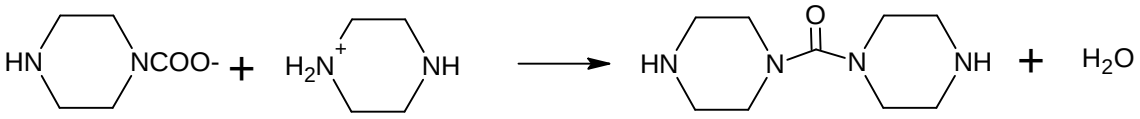

Results and Discussion

GC Experimental Results

Aqueous piperazine samples with a loading of 0.8 mol CO_2/mol PZ were placed in ovens at 120°C and 135°C and removed at weeks 1, 2, and 3. They were analyzed using the GC with a HP-5 column. Figure 6 below shows the results of this analysis.

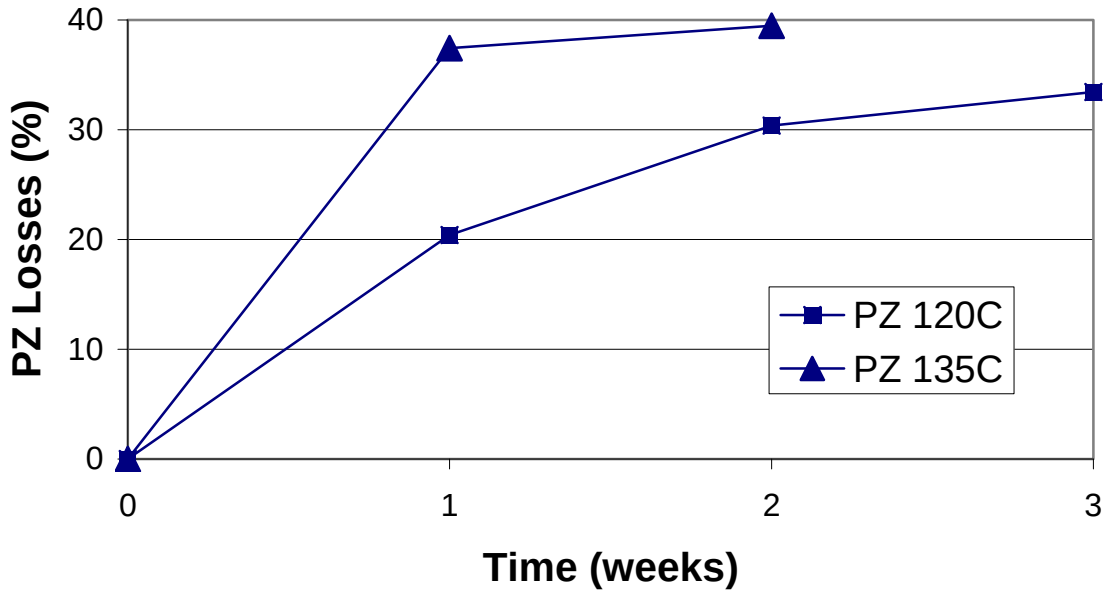

Figure 3.9.1. Piperazine losses over time at 120°C and 135°C.

These results show rapid disappearance of the PZ peak in the GC method at short times that seem to reach a chemical equilibrium within several weeks. This equilibrium seems to be temperature dependent as well since the 135°C samples showed a faster loss rate and seem to have a higher equilibrium concentration at long times. These results go against the initial prediction that PZ would not thermally degrade.

Titration Experimental Results

The total amine pH titration method showed no measurable loss in amine functionality for any of the degraded samples. This would seem to indicate that while PZ losses are evident in the GC analysis, the piperazine samples are not losing their amine functionality. This data could mean several things; 1) Piperazine is not degrading at all, but is merely an artifact of the GC conditions (i.e. high temperatures in the injection port and column coupled with sample dehydration in the sample port) 2) Piperazine thermally degrades into a compound that retains the same amine functionality as the original sample or 3) the degradation product is reversible under the titration conditions and therefore reverts back to piperazine in the titrator.

HPLC and IC Experimental Results

Comparisons of the initial sample to the degraded samples using IC and HPLC showed no losses of piperazine as well, which further validates the titration results suggesting little, if any, degradation in the piperazine system under normal stripper conditions. A HPLC chromatogram of a sample of aqueous PZ with a loading of 1 molCO_2/mol PZ that has been incubated at 135°C for 8 weeks is presented below.

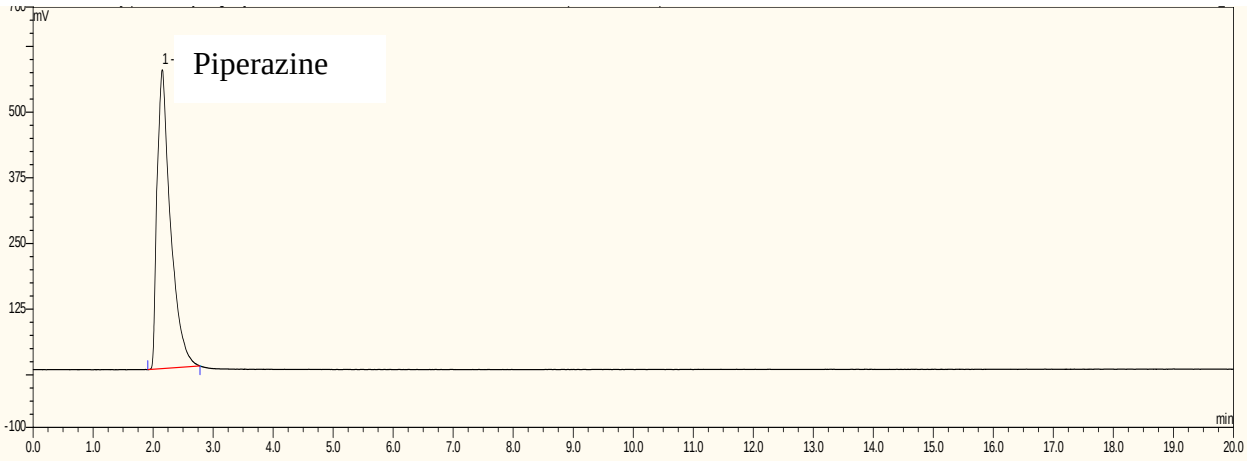

Figure 3.9.2. HPLC chromatogram of 5mPZ after 8 weeks at 135°C

As you can see, the PZ is not well retained on the HPLC column since it is very polar, but this column has been shown to separate nonpolar degradation products of MEA degradation such as

oxazolidone and HEIA. The PZ peak has little, if any, reduction in area or height over time and no additional peaks are present indicating a lack of nonpolar degradation products.

Unlike the HPLC, the cation IC can do a much better job of separating polar ionic compounds like amines. While this method will not show nonionic species, it should show any degradation products that retain their amine functionality. Below is a set of IC chromatograms of aqueous PZ incubated at 135^{o}C with a CO_2 loading of 1 mol CO_2/mol PZ at time 0, 1, 2, 4, 6, and 8 weeks.

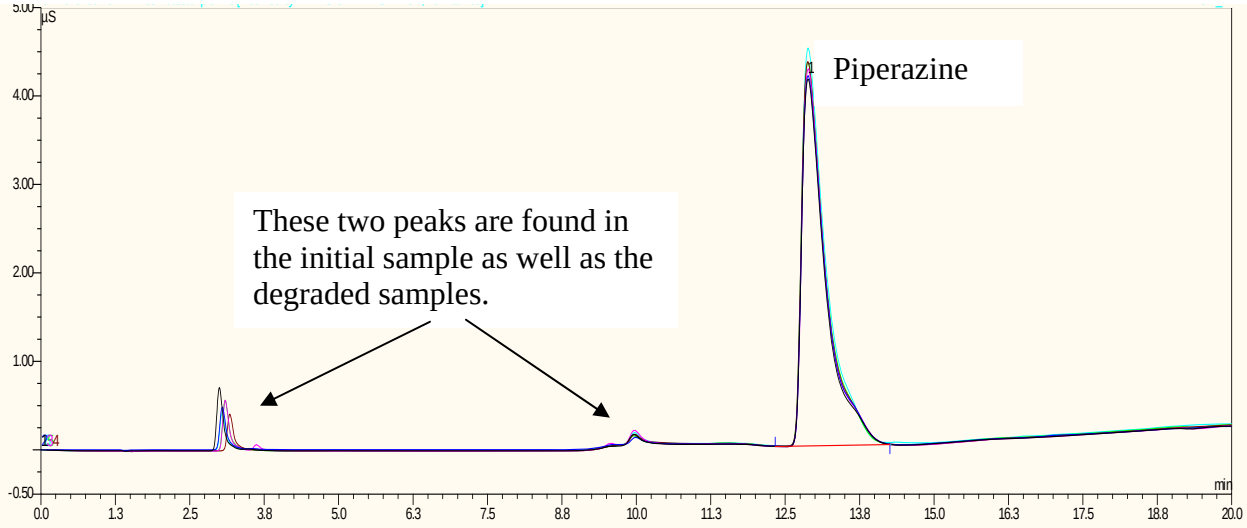

Figure 3.9.3. Overlayed IC chromatograms of aqueous PZ after 0,1,2,4,6 and 8 weeks at 135^{o}C

There is very little change in the size and shape of the PZ peak over the 8 week time span with a relative standard deviation of less than 3% for all samples. There are also no new peaks in the week 8 sample compared to the initial sample. This indicates that there is very little change in the PZ concentration, and that no new amine structures are being formed.

NMR Experimental Results

As a final test, a initial sample and degraded sample of the PZ were submitted for NMR analysis. This analysis showed nearly identical scans of both samples by C13 and proton NMR indicating that no large contaminants were present in the degraded sample.

Conclusions

The GC results showed significant degradation of the PZ samples, but titration, HPLC, IC and NMR all show little if any degradation on the same samples. The GC results only show a disappearance of the PZ peak without accounting for any degradation peaks making it impossible to show what the PZ is converting to under GC conditions. Since all of the other methods do not show any degradation, it is believed that some systematic error is associated with the GC in the injection port at 250^{o}C causing a loss of PZ introduction to the column. It was hypothesized that the degraded samples were picking up heavy metals from the stainless steel sample containers and these metals could catalyze a reaction at 250C, but initial samples spiked with nickel and chromium showed no PZ losses.

A satisfactory explanation for the GC results has not been reached, but it seems that these results are incorrect in light of the other four analytical methods results. It seems that PZ does not thermally degrade at standard stripper conditions. An additional sample was tested at 150^{o}C for over 6 weeks and was found to have little, if any, degradation by cation IC. As a comparison, 11m MEA held at 135^{o}C with a loading of 0.5 yields a 60 wt% reduction in MEA area over the same 8 week time span.

References

1. Polderman, L.D., C.P. Dillon, and A.B. Steele, *Why monoethanolamine solution breaks down in gas-treating service.* Oil Gas J., 1955. **54**(No. 2): p. 180-3.
2. Yazvikova, N.V., L.G. Zelenskaya, and L.V. Balyasnikova, *Mechanism of Side reactions During removal of Carbon Dioxide from Gases by Treatment with Monoethanolamine.* Zhurnal Prikladnoi Khimii, 1975. **48**(3): p. 674-676.

Thermodynamics of MDEA/PZ/CO_2/H_2O

Progress Report Q3, 2007
By Bich-Thu Nguyen
Luminant Carbon Mangemen Program
Department of Chemical Engineering
The University of Texas at Austin

Abstract

This work explores the volatility of MDEA and PZ in blends of varying amine concentrations at 40ºC and 60ºC. Amine volatilities are reported in terms of partial pressures and are further analyzed in terms of their apparent activity coefficients as a function of loading, temperature, and amine concentration. PZ partial pressure is found to decrease steadily as CO_2 loading, reported on a basis of mol CO_2/mol PZ, is increased. Furthermore, as expected this partial pressure is higher with respect to the higher experimental temperature and concentration. As for the apparent PZ activity coefficient, it behaves the same as the partial pressure with respect to all the experimental variables mentioned. Conversely, the apparent MDEA activity coefficient is seen to be higher with respect to the lower experimental temperature (40ºC) and also with lower MDEA concentrations.

Introduction

The objective of this work is to determine the volatility of amine species (methyldiethanolamine and piperazine) in blends of varying amine concentrations at 40ºC and 60ºC. More specifically, amine volatilities are explored in terms of activity coefficients as a function of loading, system temperature, and amine concentration

Data and Experimental Methods

The equilibrium partial pressures of CO_2, PZ, MDEA, and water were measured in a stirred reactor coupled with FTIR analysis (Figure 1).

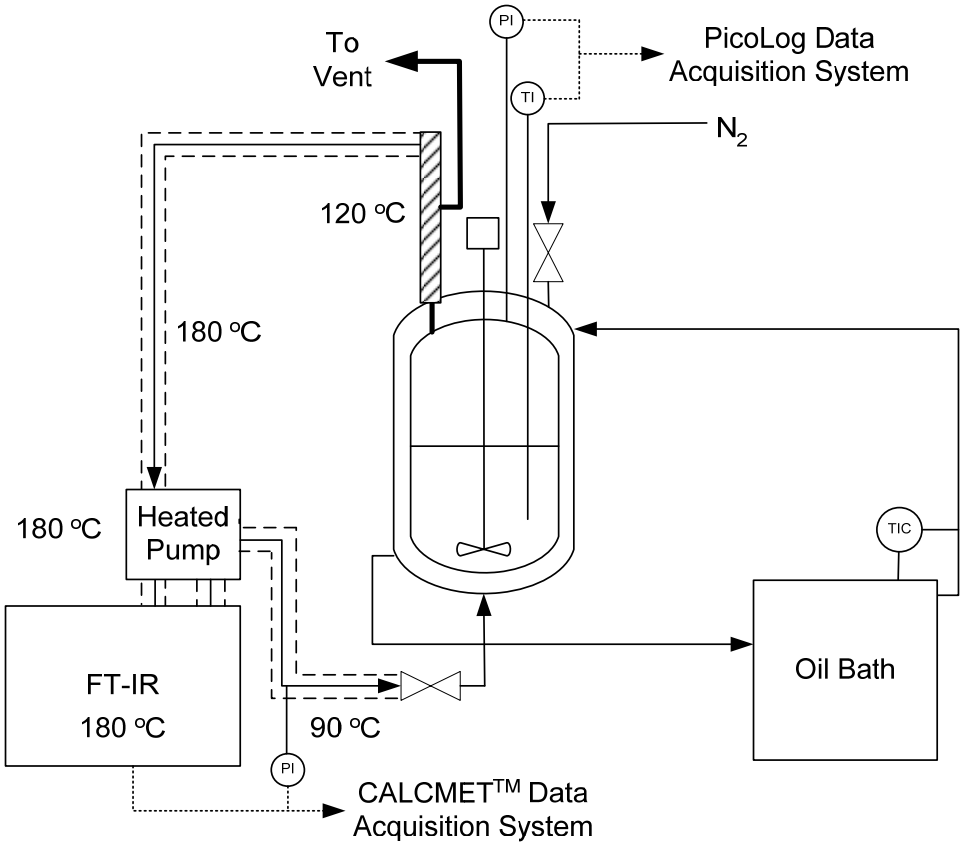

Figure 1. Schematic of Vapor-Liquid Equilibrium FTIR Apparatus

This VLE apparatus allows simultaneous measurements of CO_2 solubility and amine volatility. The heated sample is introduced at 180ºC to a hot gas FTIR at the same temperature. The elevated operating temperature serves to eliminate condensation and adsorption of vapor amine to any apparatus surface; thus, low vapor concentrations of amine can be analyzed more accurately.

The FTIR equipment has the capability of performing a multi-component analysis by combining complete calibration spectra of each component to make up the measured spectrum of the unknown gas. Once FTIR analysis is complete, gas is recycled back to the reactor at a temperature that is ~55ºC higher than the reactor temperature to preserve low amine concentrations. Note that it takes roughly 1.5-2.0 hours for the system to reach equilibrium before a data point can be taken.

Solution loading is prepared gravimetrically by weighing the total contents of the system before and after sparging with CO_2. CO_2 content of the solution is also determined by acidification and evolution into an IR analyzer. The total amine concentration in solution is determined by acid titration to an inflection point.

The below table captures all of the experimental data collected up to this point.

Table 1. Experimental Amine Volatility Data

	Solution	Loading	T (C) reactor	P (bars) reactor	yMDEA (ppm)	yCO2 (ppm)	yPZ (ppm)	yH2O (vol%)
4M MDEA/0.6M PZ (40C)	3-2	0.5	39.98	0.9875	5.2	2196	6	6.4
4M MDEA/0.6M PZ (40C)	3-3	1	39.99	0.9859	5.9	9562	2.2	6.4
4M MDEA/0.6M PZ (60C)	3-4	0	59.99	0.9862	26	3	38.8	16.6
4M MDEA/0.6M PZ (60C)	3-5	0.5	59.97	0.985	24.8	7227	17.4	16.6
4M MDEA/0.6M PZ (60C)	3-6	1	59.99	0.9845	27.1	4.4 vol%	15	16.7
4M MDEA/1.2M PZ (40C)	4-1	0	39.99	0.9884	5.7	4.1	19.3	6.1
4M MDEA/1.2M PZ (40C)	4-2	0.5	40.03	0.9862	6.6	1736	16	5.5
4M MDEA/1.2M PZ (40C)	4-3	1	39.98	0.9853	6.9	13966	4	6
4M MDEA/1.2M PZ (60C)	4-4	0	59.99	0.9841	25	2.9	66	16.4
4M MDEA/1.2M PZ (60C)	4-5	0.5	60.00	0.9841	27.8	17290	27.7	15.9
4M MDEA/1.2M PZ (60C)	4-6	1	60.01	0.9829	28.6	8.3 vol%	12.9	15.8
2M MDEA/0.3M PZ (40C)	5-1	0	40.01	0.9829	11.1	10.7	7.8	7.2
2M MDEA/0.3M PZ (40C)	5-2	0.5	39.97	0.9825	12	1859	5.8	7.2
2M MDEA/0.3M PZ (40C)	5-3	1	39.96	0.982	11	3404	4.7	7.2
2M MDEA/0.3M PZ (60C)	5-4	0	59.95	0.9863	30.8	3.1	18.1	17.9
2M MDEA/0.3M PZ (60C)	5-5	0.5	59.96	0.9849	25.3	4772	16.4	17.9
2M MDEA/0.3M PZ (60C)	5-6	1	59.99	0.9865	24.6	18306	7.4	18
2M MDEA/0.6M PZ (40C)	6-1	0	40.02	0.9853	9	4.2	7.4	7.1
2M MDEA/0.6M PZ (40C)	6-2	0.5	39.97	0.9844	9.5	1208	8.9	7
2M MDEA/0.6M PZ (40C)	6-3	1	40.02	0.984	9.2	9366	5.8	7
2M MDEA/0.6M PZ (60C)	6-4	0	59.97	0.9877	19.3	1.4	27.1	17.5
2M MDEA/0.6M PZ (60C)	6-5	0.5	59.96	0.9874	22.2	5735	16.3	17.8
2M MDEA/0.6M PZ (60C)	6-6	1	59.96	0.9872	22.5	3 vol%	17.3	17.6

Theory

PZ vapor pressure is calculated from the below equation as provided in DIPPR database:

$$P_{vap}\,(Pa) = \exp\,[A + B/T + C(\ln T) + DT^{E}] \qquad \text{where T is in degrees Kelvin}$$

Table 1 displays the values of the equation constants along with a temperature bracket applicable to the equation.

Table 1. Constants for DIPPR Model of Liquid PZ Vapor Pressure

	A	B	C	D	E	Min T (K)	Max T (K)
PZ	70.503	-7914.5	-6.6461	5.21E-18	6	379.15	638

While the temperatures explored in this experiment are outside the applicable range of this equation, it has been confirmed that this model performs satisfactorily at predicting vapor pressures in the lower temperature regime (which includes the experimental temperatures 40ºC and 60ºC). Figure 2 below is a log scale plot of the predicted PZ vapor pressure with respect to inverse temperature. Given the relative linearity of the plot in the low temperature regime, one can reasonably conclude that the model is fairly robust and consistent at predicting vapor pressure of pure PZ from 10ºC up to 450ºC (283K to 785K respectively).

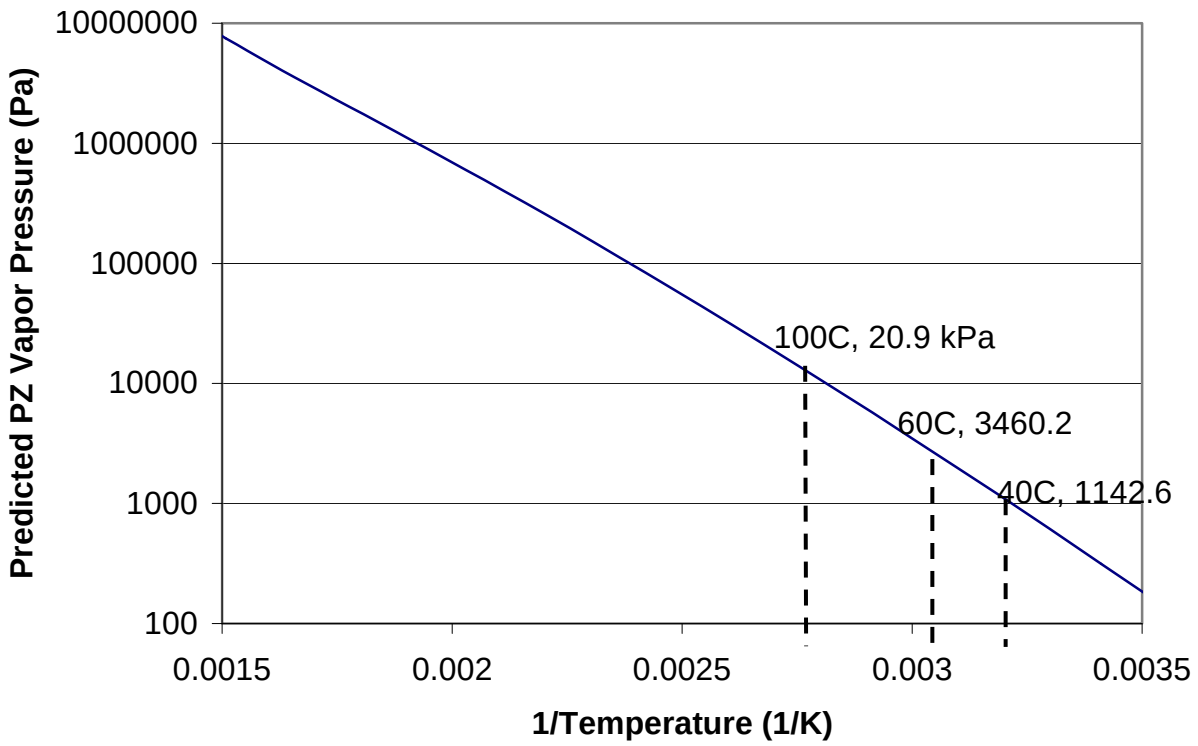

Figure 2. Predicted Vapor Pressures of Liquid PZ Using DIPPR Model

Similarly, MDEA vapor pressure can be calculated using the equation above by substituting in appropriate constants specific to this compound.

Table 2. Constants for DIPPR Model of Liquid MDEA Vapor Pressure

	A	B	C	D	E	Min T (K)	Max T (K)
MDEA	253.07	-18378.00	-33.97	2.33E-05	2.0	252.15	540

The modified Raoult's law is then used to calculate the activity coefficient for PZ:

$$\gamma_i = (y_i P) / (x_i P^o)$$

where γ_i is the activity coefficient of species i, y_i is the mole fraction of species i in vapor phase, P is the total pressure, x_i is the mole fraction of species i in liquid phase, and P^o is the pure component vapor pressure of i. Note that the activity coefficients calculated in this report are apparent values that serve as an approximation of actual activity coefficient values. The reason that only apparent values can be calculated is because x_i, the liquid mole fraction of a given amine species, reflects the total amount of that species present in the system instead of the amount of that species that is free or unreacted.

Results

Figure 3 below illustrates PZ volatility in terms of its partial pressure plotted with respect to CO2 concentration.

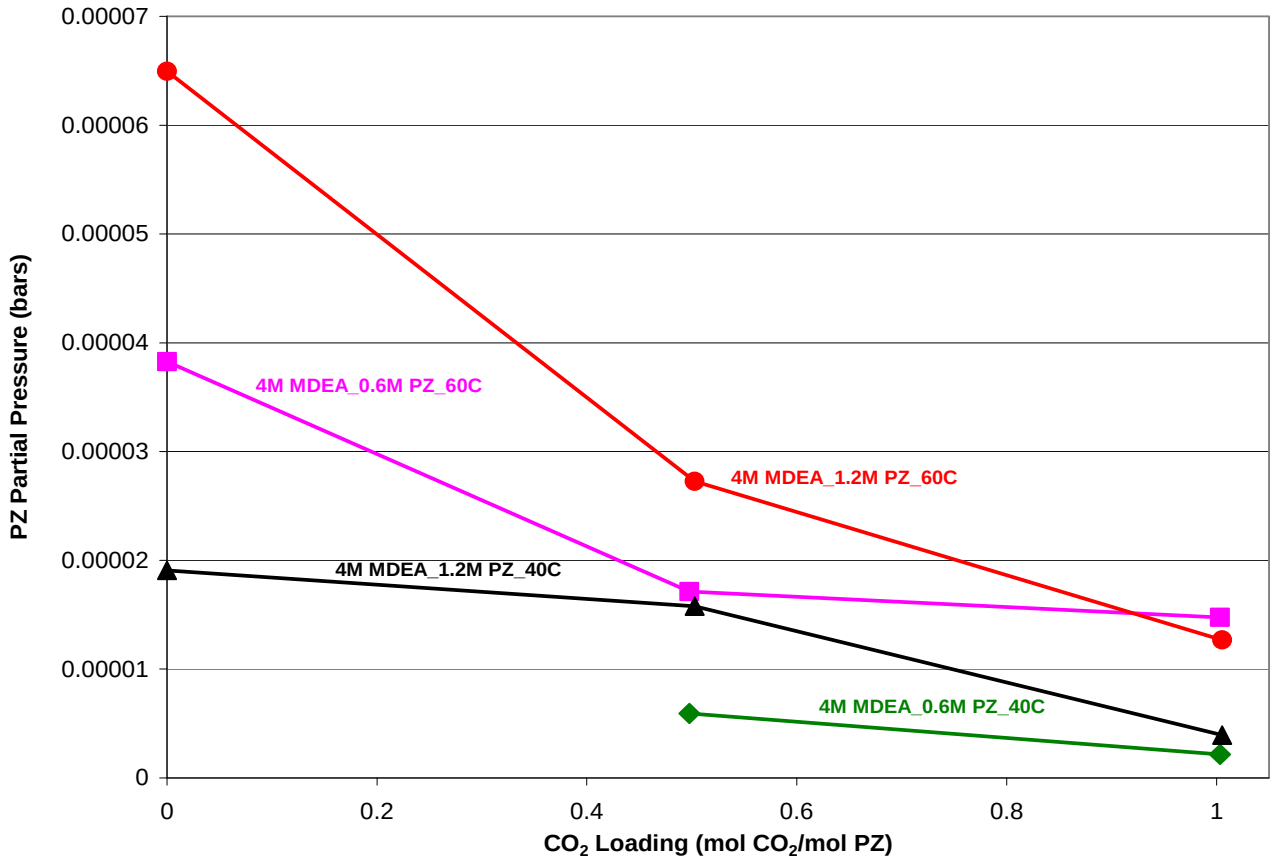

Figure 3. PZ Volatility as a Function of Loading, Temperature, and Amine Concentration

It can be seen from above that PZ partial pressure decreases steadily as CO_2 loading increases. For a given PZ concentration, it is believed that more PZ is consumed at a higher CO_2 loading as compared to a lower loading; therefore, the partial pressure of the former is expected to be lower than the latter. In addition, one also makes a note of PZ partial pressure being primarily a function of temperature. Note from above that the two series with the highest PZ partial pressures correspond to the higher experimental temperature (60ºC). Furthermore, for the same two series mentioned, the one having a higher PZ concentration (1.2M PZ) gives rise to higher partial pressures relative to the other with the lower PZ concentration.

The following figure plots the apparent PZ activity coefficient with respect to CO_2 loading.

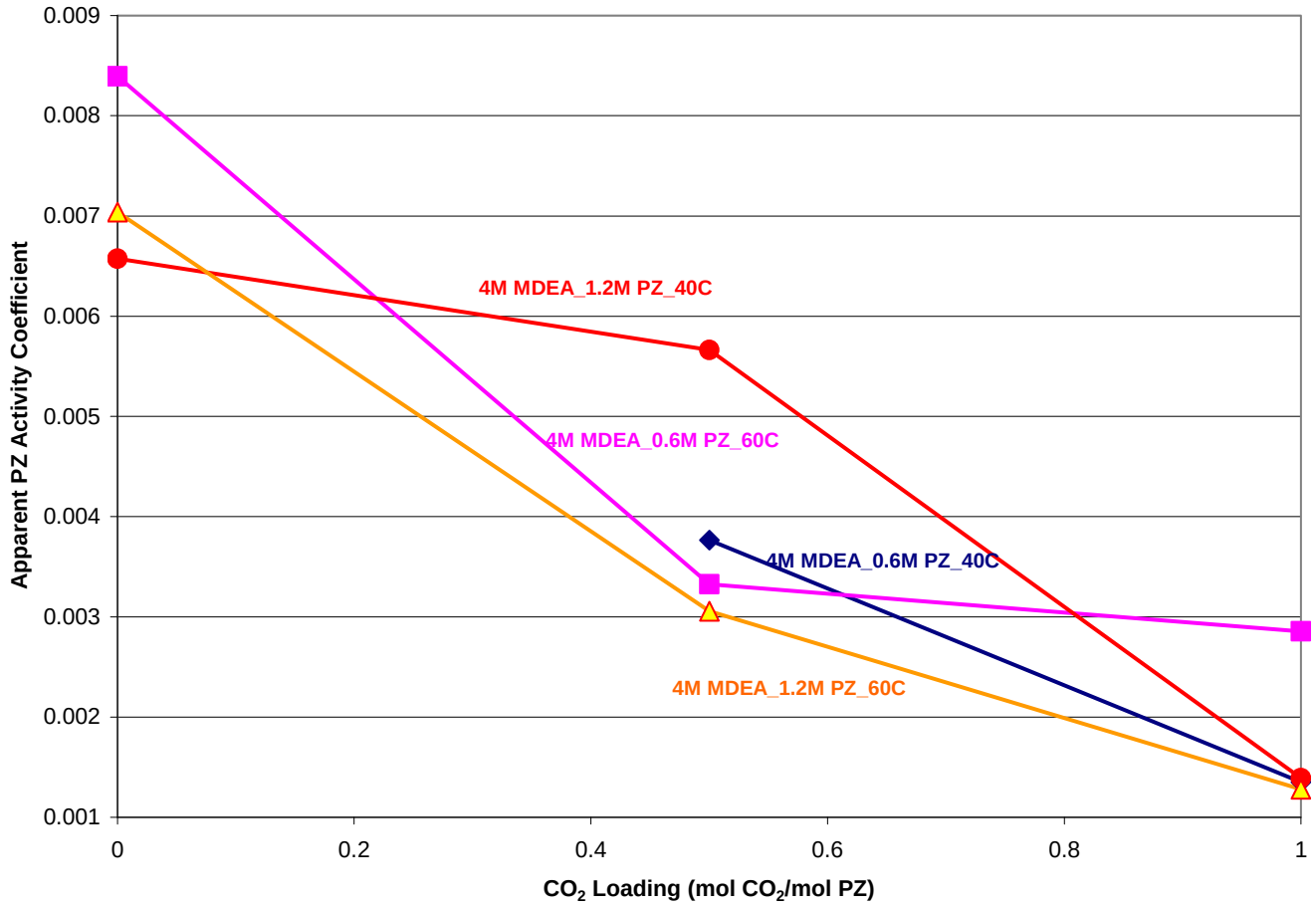

Figure 4. Apparent PZ Activity Coefficient as a Function of Loading, Temperature, and Amine Concentration

The apparent PZ activity coefficient trend with respect to CO_2 loading is similar to the partial pressure trend shown previously. As the loading increases, the apparent activity coefficient decreases steadily due to higher consumption of piperazine by CO_2. Furthermore, it is worthwhile to note that the two experimental series ran at 60ºC both show higher coefficient than those ran at 40ºC. Finally, the extremely small magnitude of the coefficient values indicates the highly non-ideal nature of PZ solution in reaction with CO_2.

A plot is also prepared to illustrate MDEA volatility as a function of CO_2 molar concentration.

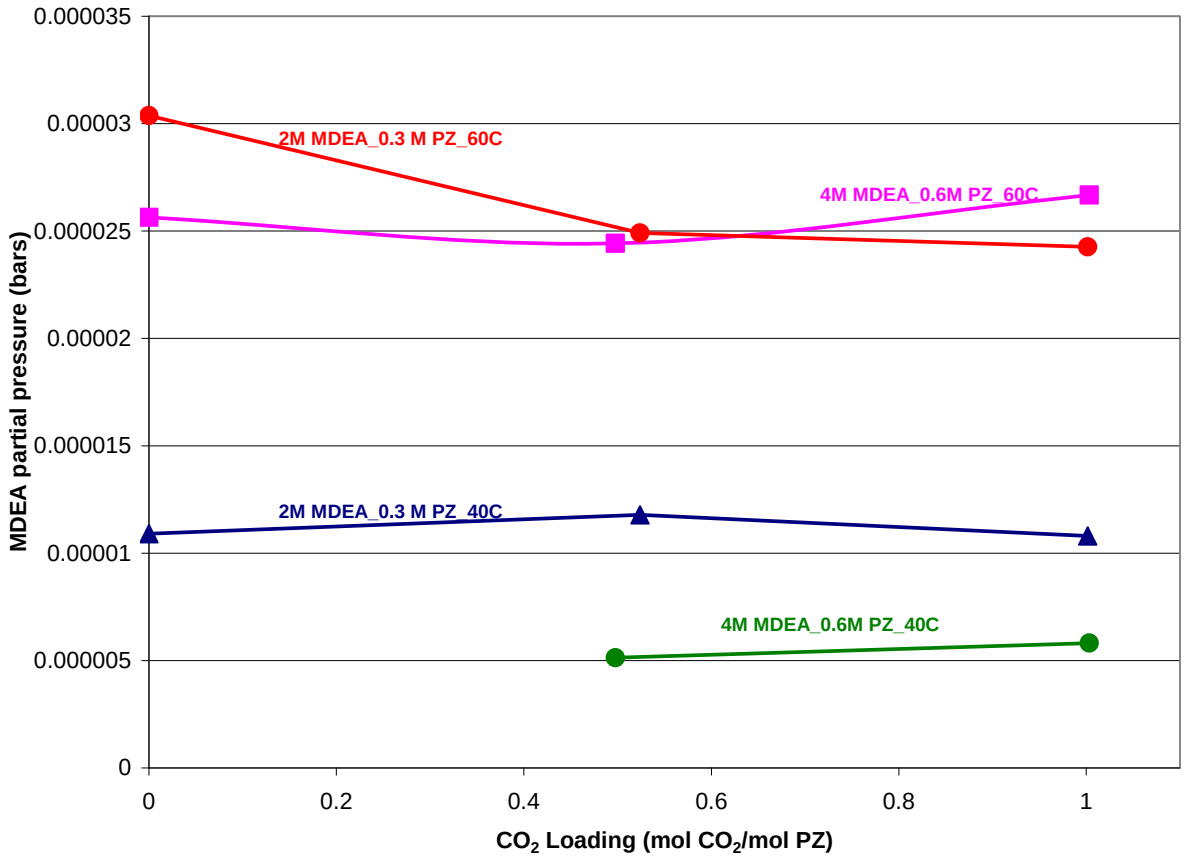

Figure 5. MDEA Volatility as a Function of Loading, Temperature, and Amine Concentration

As one can see MDEA partial pressure appears to increase slightly with an increase in CO2 loading. It is also worthwhile to make a note of MDEA partial pressure being primarily a function of temperature. Note from above that the two series with the highest MDEA partial pressures correspond to the higher experimental temperature (60C). Furthermore, for the same two series mentioned, the one having the lower MDEA concentration (2M MDEA) gives rise to higher partial pressures relative to the other with the higher MDEA concentration.

The following plot depicts the apparent behavior of MDEA activity coefficient.

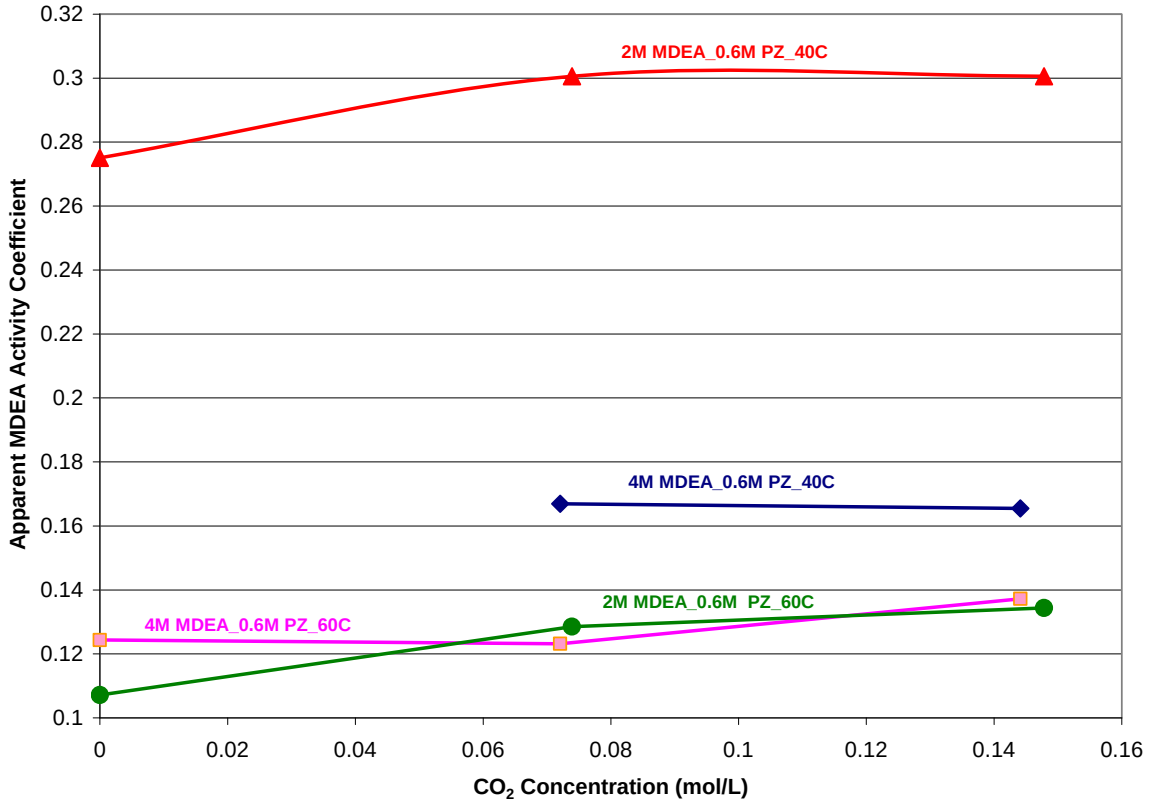

Figure 6. Activity Coefficient as a Function of Loading, Temperature, and Amine Concentration

In regard to the apparent MDEA activity coefficient, it can be seen that the two series with the highest coefficients are those conducted at the lower experimental temperature (40C). Furthermore, for the same two series mentioned, the one having the lower MDEA concentration (2M MDEA) gives rise to higher activity coefficient relative to the other with the higher MDEA concentration. It is also interesting to note that MDEA activity coefficient increases slightly as the molar concentration of CO_2 increases.

Future Work

In the near future, effort will be made to continue collecting additional data for blends of other amine concentrations. Additionally, the focus will be on exploring amine volatility in the absorber lean and wash water streams along with stripper unit. Subsequently, AspenPlus will be used to model experimental data in order to arrive at thermodynamic models for PZ and MDEA activity coefficients. Aside from exploring amine volatility, a separate effort will be made to conduct heat capacity measurements.

Influence of Liquid Properties on Effective Mass Transfer Area of Structured Packing

Quarterly Report for July 1 – September 30, 2007

October 5, 2007

by Robert Tsai

(Supported by the Luminant Carbon Management Program and by the Separations Research Program)

Abstract

The effective mass transfer area of Sulzer Mellapak 250Y structured packing has been measured via CO_2 absorption into dilute caustic solution at high (72 mN/m) and low (35 mN/m) surface tension. The results were practically identical, implying that the liquid spreadability on the packing surface was equivalent in both cases. Sessile drop contact angle data were obtained in an effort to understand and justify the observed phenomenon. Initial measurements on a textured Mellapak surface were unsuccessful, so an un-textured (smooth) stainless steel sheet was tested instead. The high and low surface tension fluids had noticeably different contact angles (70˚ vs. 40˚) on this surface. It is suspected that the observed spreading behavior was primarily dictated by the properties of the packing and not those of the liquids.

The effective mass transfer area of Koch-Glitsch Flexipac 1Y structured packing was evaluated as a function of liquid load with a viscosity-enhanced caustic solution ($\mu \sim 5.5$ mPa·s, $\sigma \sim 57$ mN/m). A comparison with the baseline data ($\mu \sim 0.8$ mPa·s, $\sigma \sim 72$ mN/m) showed that the physical property modifications had no tangible effect.

Introduction

Packing is commonly used in distillation, absorption, and stripping processes as a means of promoting efficient contact between gases and liquids. One important application of packed columns is treating flue gas for CO_2 capture. Reliable packed column mass transfer models are necessary for design and analysis purposes. A critical factor involved in modeling is the prediction of the effective interfacial area of packing (a_e), which can be considered as the total gas-liquid contact area that is actively available for mass transfer. Accurate effective area characterization is especially vital to our research efforts in CO_2 capture, because the governing mass transfer is such that packing area is the only contactor property on which the rate of CO_2 absorption depends.

Numerous empirical or semi-empirical packing area correlations have been presented in the literature, but none has been shown to be truly predictive over a wide range of conditions. Wang et al. (2005) performed a comprehensive review of the available models for both random and structured packing. The various correlations predict substantially different effects of liquid viscosity and surface tension, properties that would be expected to fundamentally influence the wetted area of packing. Thus, the role of these properties in the "creation" of area is not at all clear.

The Separations Research Program (SRP) at the University of Texas at Austin has the capability of measuring packing mass transfer areas. Measurements are performed by absorbing CO_2 from air with 0.1 M NaOH in a 460 mm (18 in) OD column. Unfortunately, physical parameters are limited to those of water, making it potentially inaccurate to extend these results to other fluids of interest, such as amine solvents, due to the differences in viscosity and surface tension.

Limited understanding of the fluid mechanics and mass transfer phenomena in packed columns has been noted, and the need for experiments over a broader range of conditions has been identified (Wang et al., 2005). The goal of this research is to address these shortcomings and ultimately develop an improved effective area model for structured packing. The general objectives are to:

- Develop a fundamental understanding of the fluid mechanics associated with structured packing operation;
- Determine suitable chemical reagents to modify the surface tension and viscosity of the aqueous caustic solutions employed to make packing area measurements, and characterize potential impacts of such additives on the CO_2-NaOH reaction kinetics;
- Expand the SRP database by measuring effective areas of structured packing over a range of liquid viscosities and surface tensions;
- Combine the theory and the data into a semi-empirical effective area model for structured packing.

Experimental

460 mm OD Packed Column

The packed column used for effective area measurements had an outside diameter of 460 mm (18 in), inside diameter of 427 mm (16.8 in), and a 3 m (10 ft) packed height. For details regarding the apparatus and experimental procedure, the Q4 2006 report or the research proposal submitted this quarter may be consulted.

Wetted-Wall Column (WWC)

The wetted-wall column (WWC) is a vapor-liquid contactor with an interfacial area of 38.52 cm^2 and is the same apparatus that Mshewa (1995), Bishnoi (2000), and Cullinane (2006) employed to measure the kinetics of various CO_2-amine systems. The auxiliary equipment and protocol associated with a standard WWC experiment are archived in earlier quarterly reports (e.g. Q3 2006) and in the research proposal.

Goniometer

The goniometer (ramé-hart Inc., Model #100-00) was equipped with an adjustable stage; the overall set up included a computer-linked camera for live image display and a light source (see Q3 2006 report). The apparatus was utilized in conjunction with FTA32 Video 2.0 software (developed by First Ten Angstroms, Inc.) to make surface tension measurements via the pendant drop method. It was also used to obtain contact angle data via the sessile drop technique. For this purpose, surfaces were thoroughly rinsed with 1% Alconox® solution, acetone, and distilled water and were dried in a clean oven. After allowing the surfaces to cool, sessile drop measurements were conducted immediately to minimize the potential for evaporation and surface contamination. DROPimage software was employed for the analysis of the drops (5μL in size).

Rheometer

The rheometer employed for viscosity measurements was first described in the Q4 2006 report. To reiterate, the apparatus (Physica MCR 300) was manufactured by Anton Paar USA. Temperature was regulated with a Peltier TEK 150P-C unit and a Julabo F25 water bath unit (for counter-cooling). Measurement profiles typically consisted of a linearly increased or decreased shear rate (100-2000 s^{-1}), with a total of 20 points recorded at 15 second intervals. Viscosity was determined from a plot of shear stress (measured) vs. shear rate.

Materials

0.1 M NaOH solution for WWC experiments was purchased from Fisher Scientific (certified grade). The solid NaOH pellets used in packed tower experiments were obtained from PHARMCO-AAPER (ACS grade, 98.5%). Surfactant (Tergitol™ NP-7) and high molecular weight poly(ethylene oxide) (POLYOX™ WSR N750,

pharmaceutical grade) were procured from Dow Chemical. Antifoam agent (Dow Corning® Q2-3183A) was supplied by Dow Corning®.

Results and Discussion

Theoretical Analysis of Data

The fundamental equation used to interpret both the packed column and WWC results is presented in Eq 1. The overall mass transfer resistance is expressed as a series relationship of the gas and liquid contributions. K_G, k_G, and k_g' respectively represent the overall, gas-side, and liquid-side mass transfer coefficients.

$$\frac{1}{K_G} = \frac{1}{k_G} + \frac{1}{k_g'} \tag{1}$$

For the WWC, the overall mass transfer coefficient is calculated from the CO_2 flux and the partial pressure driving force.

$$K_G = \frac{N_{CO_2}}{P_{CO_2\,LM}} = \frac{N_{CO_2}}{P(y_{CO_2\,in} - y_{CO_2\,out})} \ln\left(\frac{y_{CO_2\,in}}{y_{CO_2\,out}}\right) \tag{2}$$

A gas-side mass transfer coefficient correlation for the WWC was developed by absorption of SO_2 into 0.1 M NaOH, an entirely gas-film controlled process (Bishnoi, 2000). Eq 3 is a rearrangement of this correlation, which involved the Sherwood, Reynolds, and Schmidt numbers and the physical dimensions of the system.

$$k_G = 1.075\left(\frac{u_G\, d^2}{L\, D_{CO_2,G}}\right)^{0.85}\left(\frac{D_{CO_2,G}}{RTd}\right) \tag{3}$$

Eqs 1-3 are used to calculate k_g', which has been defined as a liquid-side mass transfer coefficient expressed in terms of a CO_2 partial pressure driving force.

$$k_g' = \frac{\sqrt{k_{OH^-}[OH^-]D_{CO_2,L}}}{H_{CO_2}} \tag{4}$$

For comparison, Eq 4 can be evaluated using literature correlations for the diffusivity of CO_2 in electrolyte solutions ($D_{CO2,L}$), the Henry's constant of CO_2 in electrolyte solutions (H_{CO2}), and the rate constant (k_{OH-}) (Pohorecki and Moniuk, 1988).

Eq 1 is also central to the analysis of data gathered using the 460 mm OD packed column. The gas-side resistance was intentionally limited by using dilute caustic solution (0.1 M) and operating at high air velocities (1 or 1.5 m/s). Even under the worst circumstances, this resistance (estimated using the correlation for k_G proposed by Rocha et al. (1996)) should have been accountable for no more than 1.5% of the overall mass transfer resistance. Therefore, gas-side resistance was ignored in the analysis, and K_G was assumed to be equal to k_g'. This approximation enabled the effective packing area (a_e) to be determined, by separating it from the volumetric mass transfer coefficient, $K_G a_e$, as shown in Eq 5.

$$a_e = \frac{u_G \ln\left(\frac{y_{CO_2\,in}}{y_{CO_2\,out}}\right)}{ZK_G RT} \approx \frac{u_G \ln\left(\frac{y_{CO_2\,in}}{y_{CO_2\,out}}\right)}{Zk_g' RT} \qquad (5)$$

Surface Tension Studies

Surfactants were chosen as a means of simulating low, organic-like surface tension conditions. Addition of a nonionic surfactant (125 ppm_v Tergitol™ NP-7) and antifoam agent (50 $ppm_{w/v}$ Dow Corning® Q2-3183A antifoam) to 0.1 M NaOH yielded a solution with a surface tension of approximately 35 mN/m (measured via pendant drop analysis) that exhibited minimal foaming. Interesting data were obtained when this low surface tension solution was compared with the base case solution (0.1 M NaOH) in the WWC and 460 mm OD packed column. These have been documented in previous reports and are summarized below.

- The presence of the additives had no discernible effect on the CO_2-NaOH reaction kinetics (interpreted in terms of k_g').
- The effective mass transfer area of Sulzer Mellapak 250Y structured packing (a_p = 250 m^2/m^3, low surface area / high capacity) was the same at both high and low surface tension. Fractional areas (defined as a_e/a_p) varied from approximately 0.6 to 1.1 over liquid loads of 2.4 to 85.5 m^3/m^2-h but were close to unity for the majority of liquid loads.
- The baseline fractional area of Sulzer Mellapak 500Y structured packing (a_p = 500 m^2/m^3, high surface area / low capacity) was relatively low, varying from 0.35 to 0.55 as liquid load was incremented from 2.5 to 30.5 m^3/m^2-h. Reducing the surface tension to 35 mN/m resulted in substantially greater performance. At low surface tension, fractional area increased from 0.55 to 0.8 as liquid load ranged from 2.4 to 42.8 m^3/m^2-h.

The packed column results are hypothesized to be primarily attributable to capillary phenomena. The optimum mass transfer scenario would involve the entire packing surface being coated with a thin layer of liquid. However, with a high surface tension liquid like water, "pooling" or "bridging" is likely to occur within the corrugation troughs (in meniscus form) and possibly across adjacent sheets, as seen by Green et al. (2006, 2007) via x-ray imaging. This effectively reduces the available mass transfer area. This effect, present even in low surface area packings (Figure 1), would be quite prevalent in high surface area packings, due to the greater internal density. Consequently, the advantage of having a higher geometric area is partially offset.

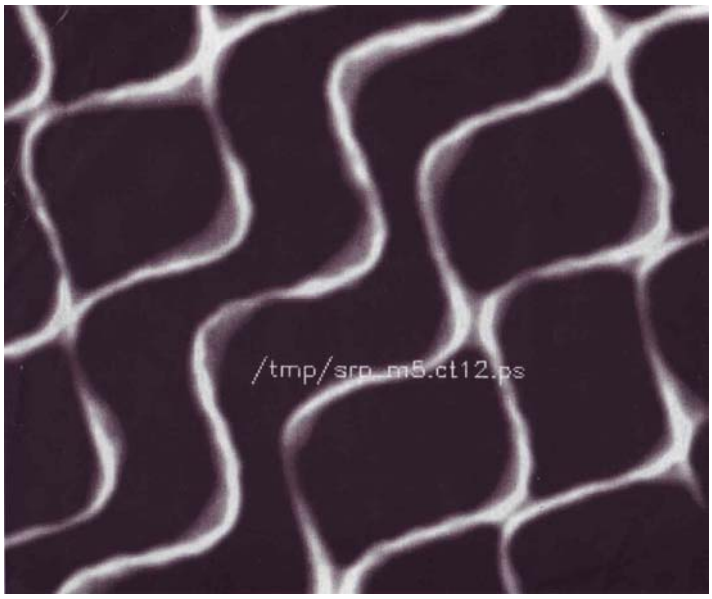

Figure 1. X-ray image of Mellapak 250Y structured packing, taken by Green (2006). Packing sheets are shown in white, and water is represented by grayish hues.

For structured packing, liquid would generally be expected to flow in the form of a film on the packing sheets (rather than free-falling droplets), with greater liquid spreading typically being associated with lower surface tension. Here, however, the effective mass transfer area of Mellapak 250Y was the same at both high and low surface tension, which indicates that the liquid spreadability was similar for both conditions for this packing and, by analogy, for the 500Y packing. This suggests that the key effect of the reduced surface tension was not improved wetting of the bulk packing internals, as one might expect, but rather, alleviation of wasteful liquid bridges and menisci. In comparison to the 250Y packing, the 500Y packing would have a considerably greater portion of its surface rendered inaccessible on account of these capillary effects at high surface tension so it should benefit much more from a decreased surface tension.

If the surface tension reduction was indeed accompanied by a decrease in contact angle – a natural presumption, as asserted by Nicolaiewsky and Fair (1999) – then the data signify that contact angle may not be as critical to the wetting of the packing surface as many models (e.g. Rocha et al., 1996) contend. However, it is also possible that the similar spreadabilities were due to the apparent contact angles being equivalent for both the high and low surface tension scenarios. Examining Young's relation (Eq 6), one could hypothesize that the presence of surfactant could have altered the solid-liquid interfacial energy in addition to the vapor-liquid interfacial energy ("surface tension") in a manner that ultimately resulted in the contact angle being balanced between the two changes.

$$\cos\theta = \frac{\sigma_{SG} - \sigma_{SL}}{\sigma} \qquad (6)$$

Alternatively, the "waffled" physical texture of the Mellapak packing could have induced appreciable wetting even at high surface tension – enough so that no further spreading occurred even when the surface tension was reduced. To test these hypotheses, contact

angle measurements were conducted via the sessile drop technique on a non-corrugated piece of sheet metal sharing the same characteristics as that of the Mellapak packing. Unfortunately, the surface features made these measurements difficult and unreliable (Figure 2); vastly different angles could be obtained depending on the drop volume and placement (i.e. within a "crest" or "valley" of the embossed surface).

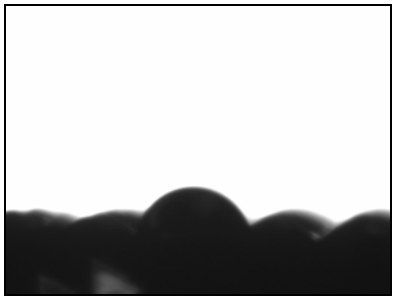

Figure 2. Water sessile drop on Mellapak surface.

As a temporary approximation to the problem, a smooth stainless steel sheet was tested instead. The contact angle data are displayed in Tables 1 and 2. Example images of the drops are shown in Figures 3 and 4.

Table 1. Contact Angle Data for 0.1 M NaOH on SS Sheet

Sample	Contact Angle (L) (deg)	Contact Angle (R) (deg)	Mean Contact Angle (deg)
1	68	72.4	70.2
2	67.9	69.5	68.7
3	76.2	83.1	79.7
4	74.6	74.1	74.4
5	74.2	72.4	73.3
6	72.5	74.4	73.5
Average	72.23	74.32	73.3
St. Dev.	3.52	4.64	3.82

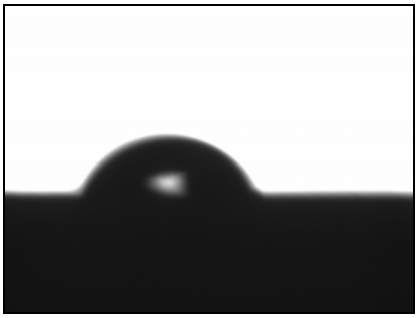

Figure 3. 0.1 M NaOH sessile drop (Sample 6 in Table 1) on SS sheet.

Table 2. Contact Angle Data for 0.1 M NaOH / 125 ppm_v Tergitol™ NP-7 / 50 $ppm_{w/v}$ Dow Corning® Q2-3183A Antifoam on SS Sheet

Sample	Contact Angle (L) (deg)	Contact Angle (R) (deg)	Mean Contact Angle (deg)
1	45.3	37.9	41.6
2	45.7	38.9	42.3
3	44.8	39.6	42.2
4	47.7	42.9	45.3
5	45.1	39.6	42.4
6	45.8	37.0	41.4
7	43.3	34.7	39.0
8	43.6	36.2	39.9
9	44.9	41.3	43.1
Average	45.13	38.68	41.91
St. Dev.	1.29	2.55	1.81

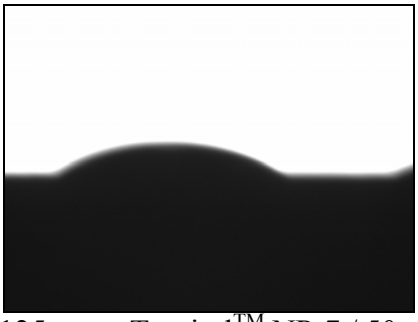

Figure 4. 0.1 M NaOH / 125 ppm_v Tergitol™ NP-7 / 50 $ppm_{w/v}$ Dow Corning® Q2-3183A antifoam sessile drop (Sample 1 in Table 2) on SS sheet.

The obtained data were useful in two regards. First, they established the anticipated reproducibility of the sessile drop technique, which was quite satisfactory (within 5˚). Furthermore, they showed that the contact angle was notably different for the base case (~70˚) and surfactant solutions (~40˚), thereby invalidating the Young's equation argument proposed above. For sheet-metal surfaces, Rocha et al. (1996) proposed Eqs 7 and 8 as a means of relating contact angle and surface tension.

$$\cos\theta = 5.211\times10^{-16.835\sigma} \qquad \text{for } \sigma > 0.055 \text{ N/m} \qquad (7)$$

$$\cos\theta = 0.9 \qquad \text{for } \sigma < 0.055 \text{ N/m} \qquad (8)$$

The measured and expected (from Eqs 7 and 8) contact angles are compared in Table 3.

Table 3. Comparison of Experimental and Calculated Contact Angles

Sample	Approx. σ (mN/m)	Expt. θ (deg)	Calc. θ (deg)
0.1 M NaOH	70.09	73.3	69.86 (from Eq 7)
0.1 M NaOH / 125 ppm_v Tergitol™ NP-7 / 50 $ppm_{w/v}$ Dow Corning® Q2-3183A antifoam	35.55	41.91	25.84 (from Eq 8)

The contact angles for the high surface tension case match up rather well. The angles for the low surface tension case, on the other hand, do not, which is not too surprising given that Eq 8 presents a fairly broad generalization.

Viscosity Studies

High molecular weight poly(ethylene oxide) (PEO) was employed as a means of enhancing viscosity. Selection was based on several desirable attributes: potency, excellent solubility in water, and no basis for reactivity – a potential problem with other viscosity enhancers such as sucrose (Vázquez, 1997).

A survey of the literature revealed a rather unique feature of dilute, aqueous polymer solutions: the limited influence of viscosity on the diffusivity of small molecules like CO_2. Based on the theory (Lohse et al. (1981), Komiyama and Fuoss (1972), and Rischbieter et al. (1996)), even for a 10-fold increase in viscosity (achieved using ~1.25 wt % PEO-300K), the impact on k_g' was expected to be marginal. Preliminary WWC tests (Figure 5) agreed with the literature findings.

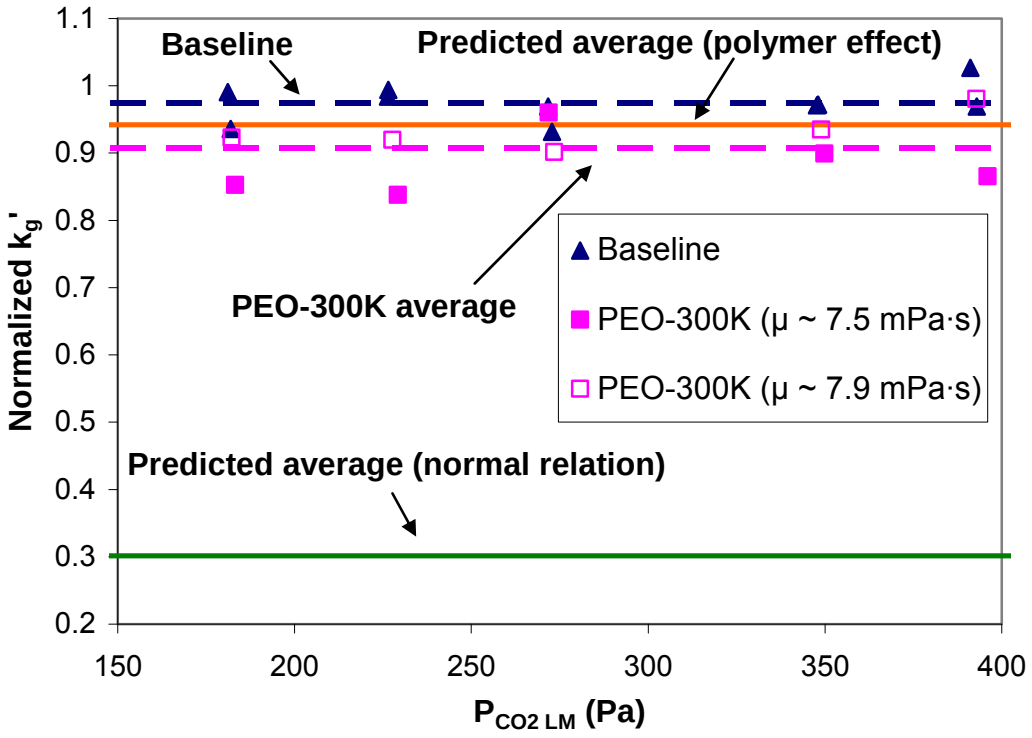

Figure 5. Normalized k_g' data for base case and high viscosity systems.

The effective mass transfer area of Koch-Glitsch Flexipac 1Y structured packing (413 m^2/m^3) was measured under both standard and high viscosity conditions (Figure 6). The properties of the high viscosity solution were roughly 5.5 mPa·s and 57 mN/m at the conditions of the experiment, and those of the base case were around 0.8 mPa·s and 72 mN/m.

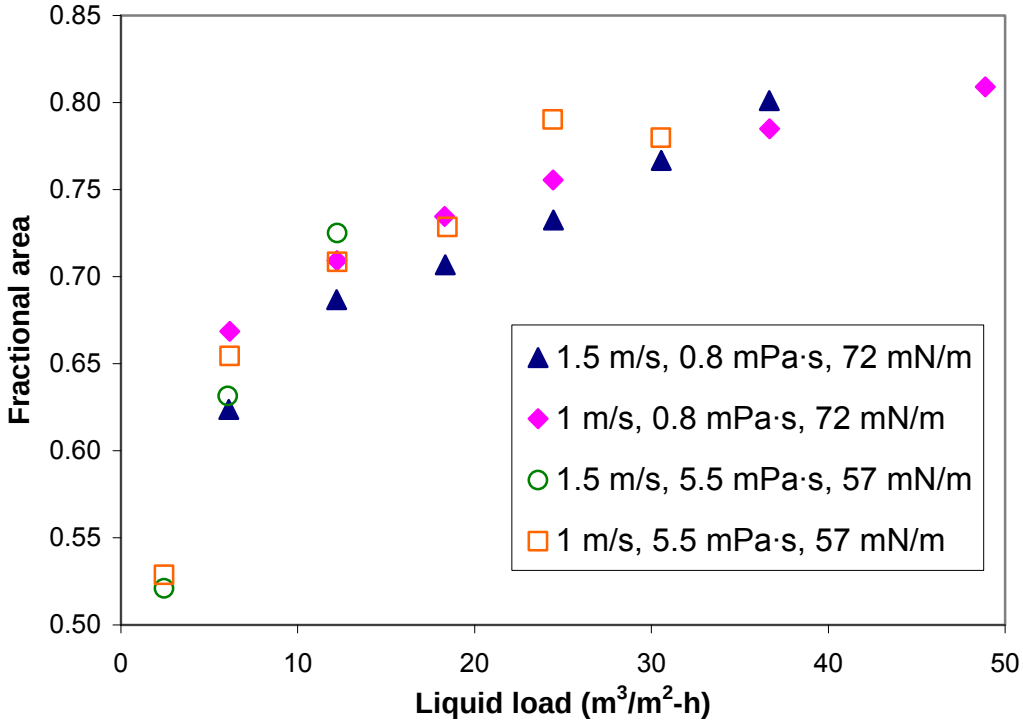

Figure 6. Fractional area measurements for Flexipac 1Y packing (a_p = 413 m^2/m^3).

For the base case, the measured fractional areas fell in between those of Mellapak 250Y and 500Y. This was expected, since the specific area of the 1Y was in between that of the two Mellapak packings. Interestingly, no appreciable difference in fractional area was observed for the high/low viscosity cases. A definitive explanation for this result cannot presently be offered, given that the theoretical effect of viscosity on mass transfer area is not at all clear. For instance, increasing the viscosity would presumably result in greater liquid hold-up, which would be beneficial for mass transfer. On the other hand, one could also argue that a higher viscosity would cause stagnation and dampen liquid rippling and turbulence (Nakajima et al., 2000). To further complicate the situation, it should be noted that the surface tension of the viscous liquid was slightly lower than the base case caustic solution, which should have increased the mass transfer area somewhat. It is possible that the viscosity and surface tension effects were either insignificant (i.e. relative to the experimental error) or perhaps happened to offset in this case. Finally, even though foaming was mostly suppressed via the addition of a minute quantity of antifoam (~2 $ppm_{w/v}$), minor foam formation could have influenced the results as well.

Conclusions

The spreading behavior of the high and low surface tension liquids on the Mellapak packing surfaces was arguably similar. The two fluids exhibited notably different contact angles (70˚ and 40˚) on a smooth, stainless steel surface, which insinuates that contact angle may be relatively unimportant in this context. This could be because the waffled

surface texture of the packing promotes good wetting regardless of surface tension. Alternatively, the physical boundaries of the packing sheets could simply limit the "improvement" in spreading that can be achieved when the surface tension is reduced. Whatever the exact reason is, a fully-wetted depiction of the structured packing, even with high surface tension fluids, could be a logical starting point for a mechanistic model.

The fractional area of Flexipac 1Y structured packing was the same for both the high viscosity and "standard" caustic solution, ranging from approximately 0.5 to 0.8 over liquid loads of 2.5 to 50 m^3/m^2-h. It is difficult to draw conclusions based on this lone data set, however, considering the various confounding phenomena that could have potentially been in effect.

Nomenclature

a_e = effective area of packing, m^2/m^3
a_p = specific (geometric) area of packing, m^2/m^3
D_{CO2} = diffusivity of CO_2, m^2/s
d = estimated hydraulic diameter of WWC reaction chamber, m
H_{CO2} = Henry's constant of CO_2, $m^3 \cdot Pa/kmol$
K_G = overall gas-side mass transfer coefficient, $kmol/(m^2 \cdot Pa \cdot s)$
k_G = gas-side mass transfer coefficient, $kmol/(m^2 \cdot Pa \cdot s)$
k_g' = liquid-side mass transfer coefficient, $kmol/(m^2 \cdot Pa \cdot s)$
k_{OH-} = second-order reaction rate constant, $m^3/(kmol \cdot s)$
L = exposed length of WWC, m
N_{CO2} = molar flux of CO_2, $kmol/(m^2 \cdot s)$
P = pressure, Pa
R = ideal gas constant, $(m^3 \cdot Pa)/(kmol \cdot K)$
T = absolute temperature, K
u = superficial velocity, m/s
$y_{CO2\ in/out}$ = mole fraction of CO_2 at inlet/outlet
Z = packed height, m

Greek Symbols
θ = contact angle, deg
μ = dynamic viscosity, $Pa \cdot s$
σ = surface tension, N/m

Subscripts
G = gas phase
L = liquid phase
S = solid phase

Dimensionless Groups
a_f = fractional area of packing, a_e/a_p

References

Bishnoi, S. Absorption of Carbon Dioxide into Aqueous Piperazine: Reaction Kinetics, Mass Transfer, and Solubility. *Chem. Eng. Sci.* **2000**, *55*(22), 5531-5543.

Cullinane, J. T. Kinetics of Carbon Dioxide Absorption into Aqueous Potassium Carbonate and Piperazine. *Ind. Eng. Chem. Res.* **2006**, *45*(8), 2531-2545.

Green, C. W. Hydraulic Characterization of Structured Packing via X-Ray Computed Tomography. Ph.D. thesis, The University of Texas at Austin, Austin, TX, 2006.

Green, C. W.; Farone, J.; Briley, J. K.; Eldridge, R. B.; Ketcham, R. A.; Nightingale, B. Novel Application of X-ray Computed Tomography: Determination of Gas/Liquid Contact Area and Liquid Holdup in Structured Packing. *Ind. Eng. Chem. Res.* **2007**, *46*(17), 5734-5753.

Komiyama, J.; Fuoss, R. M. Conductance in Water-Poly(vinyl alcohol) Mixtures. *Proc. Natl. Acad. Sci. U. S. A.* **1972**, *69*(4), 829-833.

Lohse, M.; Alper, E.; Quicker, G.; Deckwer, W. D. Diffusivity and Solubility of Carbondioxide in Diluted Polymer Solutions. *AIChE J.* **1981**, *27*(4), 626-631.

Mshewa, M. M. Carbon Dioxide Desorption/Absorption with Aqueous Mixtures of Methyldiethanolamine and Diethanolamine at 40 to 120^{o}C. Ph.D. thesis, The University of Texas at Austin, Austin, TX, 1995.

Nakajima, E. S.; Maffia, M. C.; Meirelles, A. J. A. Influence of Liquid Viscosity and Gas Superficial Velocity on Effective Mass Transfer Area in Packed Columns. *J. Chem. Eng. Jpn.* **2000**, *33*(3), 561-566.

Nicolaiewsky, E. M. A.; Fair, J. R. Liquid Flow over Textured Surfaces. 1. Contact Angles. *Ind. Eng. Chem. Res.* **1999**, *38*(1), 284-291.

Pohorecki, R.; Moniuk, W. Kinetics of Reaction Between Carbon Dioxide and Hydroxyl Ions in Aqueous Electrolyte Solutions. *Chem. Eng. Sci.* **1988**, *43*(7), 1677-1684.

Rischbieter, E.; Schumpe, A.; Wunder, V. Gas Solubilities in Aqueous Solutions of Organic Substances. *J. Chem. Eng. Data*. **1996**, *41*(4), 809-812.

Rocha, J. A.; Bravo, J. L.; Fair, J. R. Distillation Columns Containing Structured Packings: A Comprehensive Model for Their Performance. 2. Mass-Transfer Model. *Ind. Eng. Chem. Res.* **1996**, *35*(5), 1660-1667.

Vázquez, G.; Chenlo, F.; Pereira, G. Enhancement of the Absorption of CO_2 in Alkaline Buffers by Organic Solutes: Relation with Degree of Dissociation and Molecular OH Density. *Ind. Eng. Chem. Res.* **1997**, *36*(6), 2353-2358.

Wang, G. Q.; Yuan, X. G.; Yu, K. T. Review of Mass-Transfer Correlations for Packed Columns. *Ind. Eng. Chem. Res.* **2005**, *44*(23), 8715-8729.

Modeling of CO_2 Absorption by Aqueous Amines

3rd Quarter Progress Report 2007

by Jorge M. Plaza

Supported by the Luminant Carbon Management Program

Department of Chemical Engineering

University of Texas at Austin

ABSTRACT

Intercooling has been proposed as an alternative to increase absorber performance in the capture of CO_2. Analysis has been done on 11 *m* MEA and 4.5 *m* K_2CO_3/4.5 *m* piperazine absorbers using a double matrix stripper. In this quarter the effect of loading in the lean feed was evaluated for a simple absorber using the latter solvent. Complete analysis of the effect of intercooling at different loading conditions allowed the determination of an optimum bracket for the implementation of this alternative. This optimum is related to the position of the temperature bulge within the absorber. All of the results from the intercooling analysis were gathered and a first article draft has been written and is attached to this report. Future work will focus on the development of an MEA absorber model.

Description

During this period work was continued to assess the use of intercooling to improve absorber performance. The goal was to analyze the effect of loading changes in the lean feed on rich loading and solvent capacity. This analysis was done only for the 4.5 *m* K_2CO_3/4.5 *m* piperazine solvent. The MEA solvent studied previously was not considered due to the similar characteristics of both solvents. A simple absorber was set up in Aspen Plus® using the same conditions as the runs for the double matrix system. Intercooling was placed in the middle of the column and at the optimum point (minimum amount of solvent for the level of lean loading). Solvent capacity, defined as kg of CO_2 absorbed per kg of solvent, was plotted along with rich loading against lean loading. Results showed that intercooling can boost absorber performance for systems with around 0.27 to 0.38 CO_2 loading for the lean feed. This corresponds to the presence of the temperature bulge towards the middle of the column. These results, along with the previous work with the double matrix configuration, were included in an article that has been prepared for publication. The article also contains a brief description of the assumptions and conditions set up for the 4.5 *m* K_2CO_3/4.5 *m* piperazine absorber model. This is the main work product of this period and is attached to this report.

Future Work

A new absorber model will be developed for the MEA-Water-CO_2 system. It will include the new thermodynamic model developed by Hilliard (2007) and recent observations on kinetics and properties of this system by Dugas (2007) Kinetics will be represented using a simpler set of reactions that include the following:

$$2\ MEA + CO_2 \rightarrow MEAH^+ + MEACOO^- \quad (1)$$

$$MEAH^+ + MEACOO^- \rightarrow 2\ MEA + CO_2 \quad (2)$$

$$MEA + CO_2 \rightarrow HCO_3^- + MEAH^+ \quad (3)$$

$$MEAH^+ + HCO_3^- \rightarrow MEA + CO_2 \quad (4)$$

Forward kinetics for carbamate formation will be determined using an approach similar to the one developed by Dugas in IFP. Reverse rates will be calculated using equilibrium constants extracted from thermodynamic properties obtained using Hillard data.

Kinetics for formation of bicarbonate will be revised along with carbon dioxide diffusion coefficients and Henry's constants. The goal is to evaluate the importance of bicarbonate formation in CO_2 absorption modeling.

Recently available Pilot Plant data will be modeled in Aspen Plus® with a model that uses Ziaii (2006) kinetics and Hilliard developed thermodynamics. Later, this data will be used to validate the model resulting from the proposed work.

Finally, work will be conducted to assess and compare the performance of 35-40 % wt. MEA with respect to the commonly used 30 % wt.

References

Dugas. R. Personal communication on October 8, 2007.

Hilliard M., Ph.D. Dissertation (in progress). University of Texas at Austin. 2007.

Ziaii, S. "CO_2 Removal with 7m monoethanolamine MEA – AspenPlus® model for base case" - 3rd Quarter Progress Report, 2006. University of Texas at Austin.

Modeling Stripper Performance for CO_2 Removal

3rd Quarter Progress Report 2007

by David Van Wagener

Supported by the Industrial Associates Program in CO_2 Capture and Luminant Carbon Management Program

Department of Chemical Engineering

University of Texas at Austin

Abstract

A model was developed in Aspen Plus® which collated the entire absorption/stripping process for CO_2 removal using $4K^+$/4 PZ into one simulation, and it was optimized to require a minimum equivalent work. The double matrix stripper configuration was used for the stripping section, and the simulation was also compared to a simple stripper baseline. Removal of CO_2 and subsequent compression to 10 MPa required 39.7 kJ/mol CO_2 and 42.0 kJ/mol CO_2 for the double matrix and simple stripper arrangements, respectively. Previous research projected that the savings using a double matrix stripper would be 5.8 kJ/mol CO_2, more than double what this work suggests. This difference is attributed to the non-optimal lean loading used in previous research, which increases the difference between double matrix and simple stripper performance due to the system's high sensitivity to lean loading. This quarter's work also determined that the previously used five degree hot side approach for the heat exchangers is infeasible because a temperature crossover exists. A five degree cold side approach must be used, which corresponds to a ten degree hot side approach for this case.

Introduction

Previous work by Oyenekan developed stripper and compression sections in Aspen Custom Modeler (ACM). Multiple stripper configurations were evaluated, and the most energy efficient was found to be the double matrix arrangement (Oyenekan, 2006). Earlier this year, the double matrix ACM model was utilized in conjunction with an absorber model in Aspen Plus® produced by Plaza. Overall system results were generated by settling on rich and lean loadings that the absorber could realistically handle. The stripper and compression sections were optimized using these loadings, and a semi-lean composition and flow rate were calculated. The absorber and cross exchange sections were then modeled to determine the absorber properties as well as heating and pumping duties in the exchange section. These results were submitted to Trimeric for economic analysis. A goal was then set to develop a double matrix stripper model in Aspen Plus® to integrate with the absorber and cross exchange sections in one complete model.

Methods

Stripper and compression sections developed in Aspen Plus® were imported into the absorber model developed by Plaza (2006). The absorber utilized intercooling to 40°C in two stages to increase the reaction rates. The absorber model also included the cross exchange section. The only stream in the flowsheet which was not recycled to the absorber after the cross exchange was the lean stream. The recycle was essentially balanced by including a design specification which balanced the CO_2 flow entering the absorber and returning from the stripper. The complete flowsheet is shown in Figure 1.

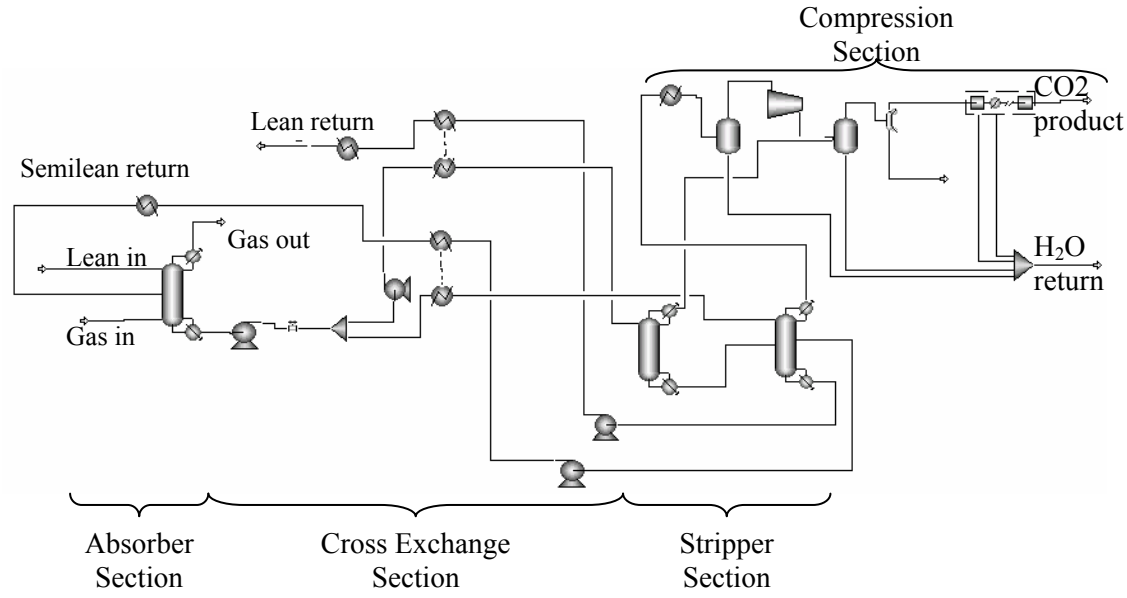

Figure 1: CO_2 Removal Configuration with Double Matrix Stripper

Debugging

A major change made to the stripper section after integration with the absorber was the final compression pressure for the multistage compressor. Initially the compressor was designed to compress to 10 MPa, but this pressure was above the critical pressure for CO_2, and the model often crashed while attempting to perform the flash calculations in this region. The compressor was then specified to only reach 1 MPa, a subcritical pressure, which enhanced the stability of the simulation. Another contributor to instability of the multistage compressor was the presence of piperazine in the vapor. The model calculated that there would be some solvent volatility, but in reality there would be no piperazine in the vapor phase. Therefore, a block was added preceding the compression train to remove piperazine from the overhead vapor from the strippers. Another stabilization technique used for the model was replacing the cross exchangers. In the process of converging the design specifications in the model, Aspen Plus® would often guess or calculate a low outlet temperature for one of the heat exchangers which occasionally resulted in a temperature crossover. The program would attempt to recover, but the errors snowballed until a fatal error occurred. Substituting each heat exchanger for a heater and a cooler with a heat stream from the cooler to the heater simulated a cross exchanger and allowed for temporary temperature crossover during convergence, thus preventing errors. The new optimized flowsheet did not yield temperature crossovers in the final results.

In addition to the configuration with the intercooled absorber and double matrix stripper, an alternate flowsheet was constructed using an absorber with no intercooling and a simple stripper. This simplified process was to be used as a "worst-case scenario" to compare to the performance of the more advanced configuration.

Design Specifications and Calculations

The lean loading, among several other variables, was an input specification for the flowsheet. There were also a number of specifications designed to achieve the desired results for the system:

1. Achieve 90% removal in the absorber with 15 meters of packing by varying the liquid flow rate into the absorber.
2. Achieve equal CO_2 flow in the stripper and absorber lean streams by varying the duty of the low-pressure stripper reboiler.
3. Achieve equal reboiler temperatures in the two strippers by varying the reboiler duty of the high-pressure stripper.
4. Achieve a cold side five degree approach in the lean exchanger by varying its cold stream outlet temperature, which feeds to the high-pressure stripper.
5. Achieve a cold side five degree approach in the semilean exchanger by varying its cold stream outlet temperature, which feeds to the low-pressure stripper.

After the model converged, the total equivalent work was calculated from the work requirements of the reboilers, pumps, and compressors. The equivalent work was minimized by finding the optimal lean loading, high-pressure stripping pressure, and split ratio. The simple stripper flowsheet was only optimized using the lean loading because the rich solving stream is not split and stripping only takes place at the base pressure of 160 kPa.

Results

Table 1 compares the optimized cases for the double matrix and simple stripper flowsheets. The table displays the optimal values of the variables for separation as well as the equivalent work for the subsequent compression to 1MPa and 10MPa. The savings from using a double matrix stripper section and intercooling in the absorber over a simple stripper and no intercooling when compressing to 1MPa and 10MPa is 6.6% and 5.3%, respectively.

Table 1: Comparison of Equivalent Work of Double Matrix Stripper with Intercooled Absorber and Simple Stripper with No Intercooling in Absorber

	Matrix	Simple
Lean Loading (mol CO_2/molalk)	0.385	0.397
Pressure (kPa)	265	-
Split	0.305	-
Equivalent Work (kJ/gmol CO_2, to 1MPa)	31.48	33.71
Equivalent Work (kJ/gmol CO_2, to 10MPa)	39.73	41.96

The sensitivity of the total equivalent work to each of the variables was also calculated. Table 2 shows the sensitivity of each variable for both cases in the form of a dimensionless second derivative, where χ_i is the variable in question normalized by the optimum value of the variable.

Table 2: Sensitivity of Equivalent Work to Optimization Variables Expressed As $\frac{d^2W}{d\chi_i^2}$

χ_i	Matrix	Simple

Lean Loading (mol CO_2/molalk)	352	430
Pressure (kPa)	7.89	-
Split	1.96	-

In the double matrix case, the equivalent work is much more sensitive to relative changes in loading compared to the pressure and split. Split ratio has a definite optimum, but the optimum is very flat. The sensitivity of the equivalent work to the variables in the double matrix case is expressed visually in Figure 2, plotting the equivalent work as a function of the three normalized optimization variables. When the loading drifts away from the optimum, the equivalent work increases much more drastically than the pressure and split ratio.

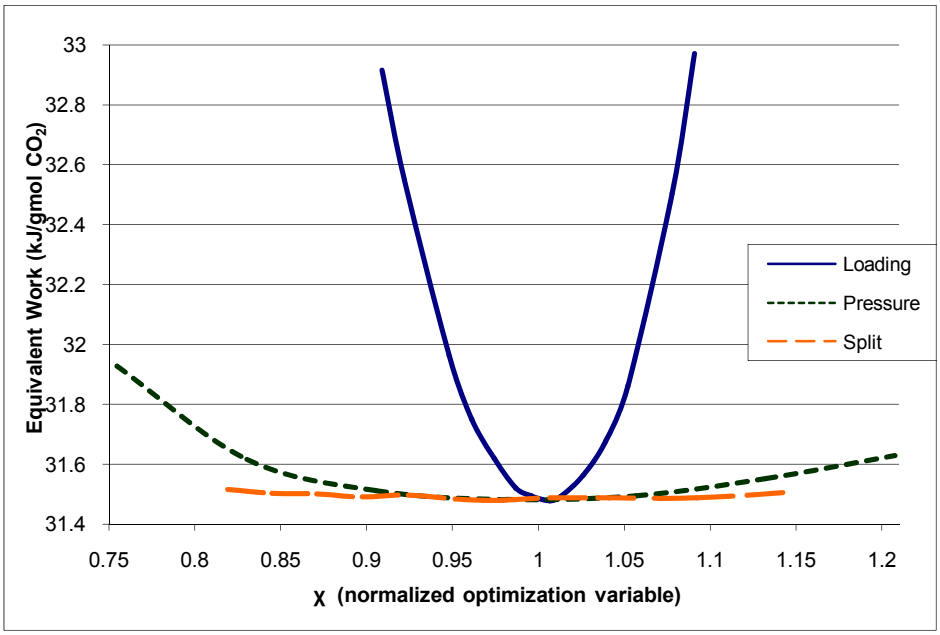

Figure 2: Comparison of Sensitivity of Equivalent Work to the Optimized Variables (4m K^+/4m PZ, intercooled absorber, double matrix stripper, compression to 1MPa)

This work also assessed the accuracy of previous simulations, which only included the stripper section. The previous simulations specified a hot side temperature approach since the heat exchangers were not modeled. This fully comprehensive model quantified the difference between using hot side and cold side approaches. The two cases for the main flow heat exchanger are presented in Table 3.

Table 3: Total Equivalent Work and Exchanger Profile with Five Degree Approach Specified on Hot Side vs. Cold Side (compression to 1MPa)

	Cold Side	Hot Side
Equivalent Work (kJ/gmol CO_2)	31.49	27.49
Lean out (°C)	46.0	40.4
Rich in (°C)	41.0	41.0
ΔT_1 (°C)	5.0	-0.6
Lean in (°C)	107.4	107.4
Rich out (°C)	97.2	102.4
ΔT_2 (°C)	10.2	5.0

The base pressure of 160 kPa was suggested from previous work because non-vacuum stripping works better for solvents with high heats of absorption such as 4m K+/4m PZ. In this

work, the base pressure in the simple stripper model was varied to determine if 160 kPa is the ideal condition. This analysis is displayed in Figure 3.

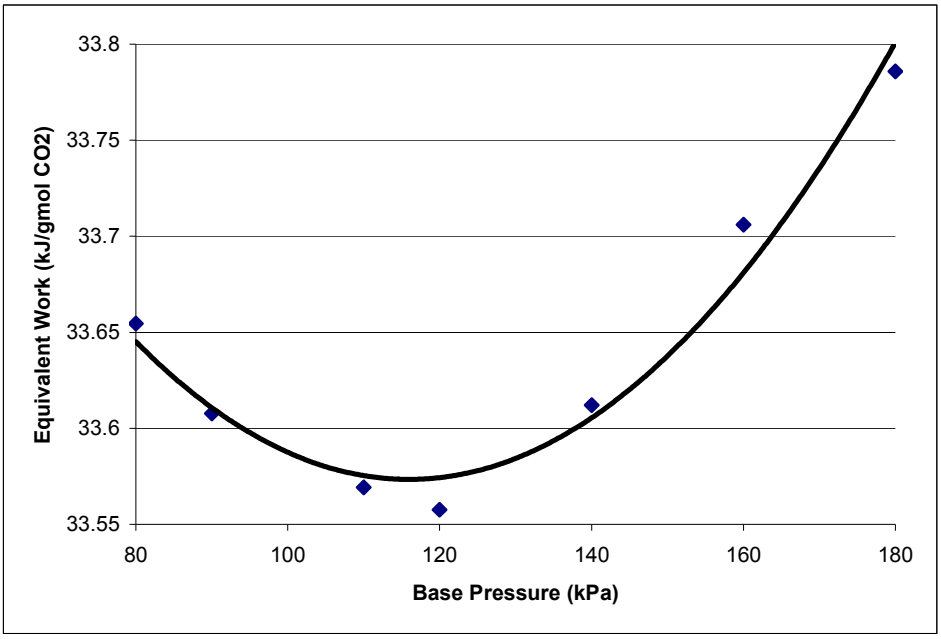

Figure 3: Effect of Base Pressure on Equivalent Work (4m K^+/4m PZ, non-intercooled absorber, simple stripper, compression to 1MPa)

The optimum equivalent work occurred using a base pressure of 120 kPa, but the work requirement only decreased by 0.44% from the work at 160 kPa. There was a definite decrease in equivalent work; however, the change was not significant compared to the previous value using 160 kPa.

Conclusions

The comparison of the performances of the double matrix stripper and simple stripper flowsheets demonstrated that there is not a drastic difference between the two configurations. Initial analysis of the double matrix configuration boasted an improvement over the simple stripper configuration of 5.8 kJ/mol CO_2 (Oyenekan, 2006), but this work suggests the improvement is only 2.3 kJ/mol CO_2. The probable explanation for the diminished improvement is a difference in the lean loading. The initial comparison between the configurations used a lean loading corresponding to an equilibrium partial pressure of CO_2 at 40°C of 0.75 kPa, but this work found optimal lean loadings which corresponded to a CO_2 partial pressure of about 0.5 kPa. Figure 2 demonstrates that the equivalent works of the systems are highly sensitive to the lean loading, especially in the simple stripper configuration. Increasing the loading would increase the equivalent work for the simple stripper case more than the double matrix case, so the difference between the two cases would be more significant. Unfortunately, this result means the double matrix configuration is not as great as once thought, but it still results in a noticeable improvement of the equivalent work.

The analysis of the implications of specifying either a hot side or cold side approach revealed that hot side five degree approaches are infeasible. The change in composition of the solvent after passing through the stripper section changes its heat capacity, and the flow is also smaller. Cross exchanging the rich stream with the lean stream, therefore, yields unequal temperature changes in the two streams. The five degree cold side approach is feasible, but it

corresponds to a ten degree hot side approach, previously shown to be less efficient than a five degree hot side approach. The five degree hot side approach, however, is not practical because it produces a temperature crossover. The equivalent work decreases with lower temperature approaches, but the size and cost of upgrading to an exchanger to achieve a lower temperature approach would raise costs dramatically.

Finally, the results from changing the base stripping pressure in the simple stripper configuration demonstrated that there are further possible savings in the equivalent work. If the base pressure were added to the list of optimization variables for the double matrix stripper analysis, the work requirement could potentially decrease as in the simple stripper case, but this work suggests that the change would be small. It has been hypothesized that the optimum case for the double matrix stripper configuration will have the same pressure ratio as this work (265 kPa/160 kPa). Equivalent pressure ratios should yield similar flashing, lost work, and compression cost contributions, so an optimum case is projected always to have the same pressure ratio.

Recommendations

A new, more accurate VLE model has been developed for MEA by Hilliard (2007?), and new models for K^+/PZ and PZ are eagerly anticipated by the same author. The new MEA model will be used to evaluate a similar system model to this work, and its results will be compared to those of a recent pilot plant run. The new K^+/PZ and PZ models will be used in conjunction with the results from this quarter's work. The changes in the results using the K^+/PZ model will be evaluated, and potential improvements in performance will be investigated using a PZ solvent.

Work on a novel stripper configuration is also commencing. The stripper section will consist merely of a large preheater and a series of flash tanks with decreasing pressure and temperature. The vapor is collected and compressed to sequester the CO_2, and the resulting liquid stream is recycled to the absorber section. This configuration has potential applications in solar-assisted stripping, where the energy for the preheater is provided by solar-generated steam. This arrangement thereby eliminates the loss of coal-generated steam from the power plant to run the stripper reboilers.

A long-term goal is to understand the mass transfer mechanisms in the stripping section. This knowledge could be used to develop more energy efficient strippers.

References

Oyenekan, B.A. and G.T. Rochelle. “Alternative Stripper Flow Schemes for CO_2 Capture by Aqueous Amines.” *AIChE J*. forthcoming.

Oxidative Degradation at Stripper Conditions

Oxidation-Reduction Potential

3rd Quarter Progress Report 2007

by Fred Closmann

Supported by the Luminant Carbon Management Program

Department of Chemical Engineering

University of Texas at Austin

Abstract

The research group has performed basic oxidation-reduction potential (ORP) experiments in order to assess the viability of using commercially available off-the-shelf ORP measurement equipment. We have measured ORP in ROC20 solutions under aerated and agitated conditions as well as quiescent conditions in a jacketed glass reactor maintained at 53.5°C. Our work has determined that the ORP of aerated systems varies with the amount of agitation and aeration in the system. In the presence of metals species (Cu^{2+}), ORP of solution immediately increased, while viscosity increased after three weeks of sitting idle. Practical findings included: (1) the presence of metals species in ROC20 at 0.01 mmolar increased the ORP of solution, and (2) commercially available ORP measurement equipment for the water industry can be adapted for amine solvent studies in the laboratory. Increases in viscosity to over 300 cP in a ROC20 solution may be evidence of polymerization of solvent after sitting idle, but no evidence of dimerization was found through basic cation exchange chromatography.

Introduction and Objectives

Over the last quarter, we have performed experiments to investigate the oxidation-reduction potential (ORP) of aqueous amine solutions with a focus on ROC20. The primary objective of the experimental work was to assess the viability of making ORP measurements of amine solutions using standard off-the-shelf equipment and methods. Knowledge of ORP in these solutions will enable the group to better understand the potential for oxidative degradation of amines to occur in the absorption/stripping process. Secondary objectives include the assessment of how ORP changes with reactor configuration changes, the repeatability of ORP measurements, and the durability of the associated equipment. Our ability to create a ROC20 solution was tested using a standard stepwise methodology commonly used by the Rochelle group. The data presented in this report was collected from the initial steps associated with a series of experiments described in the Future Work section of this report.

A solution of ROC20 was created with the intent to determine an upper limit of amine solubility at conditions mimicking loaded absorber conditions for CO_2 capture purposes. Variables including temperature and CO_2 loading were utilized in the experimental work to achieve conditions likely to occur in pilot and full-scale operation of an absorber/stripper configuration utilizing ROC20 for CO_2 removal.

Oxidation-Reduction Potential (ORP) Measurements

ORP measurements in aqueous amine solutions were made with a simple off-the-shelf ORP probe. To the extent possible, the ORP measurements were conducted following ASTM Method D1498-07 (Standard Test Method for Oxidation-Reduction Potential of Water). The group obtained an Accumet 13-620-81 probe for performing the ORP measurement studies. This probe is a platinum Ag/AgCl combination electrode (with reference) designed for measurements of ORP in aqueous solutions, and is being used in conjunction with an Altex 41 pH meter (or Cole-Parmer equivalent). To date, the equipment configuration has successfully measured ORP in ROC20 solutions.

Reactor Set-up

A jacketed glass reactor with a nominal capacity of approximately 350 ml was used in this experiment. The jacket side of the reactor was fitted with flexible tubing to a Lauda E100 circulating temperature control water bath; jacket side temperature was set at 55°C. The reactor lid was fitted with rubber stoppers sized to allow entry of the ORP probe, thermometer, and a hard plastic aeration line fitted to a compressed air supply. Air was passed through a rotameter before entering the reactor to record sparge rate; the air discharge was set at approximately one inch below the amine solution surface to maximize oxygen transfer with the given reactor configuration. The reactor was stirred with a magnetic stir bar, and the glass reactor was placed directly on a magnetic stir plate.

After start-up, we observed that the reactor set-up provided poor mass transfer of oxygen into the ROC20 solution. Modifications were made to the reactor design including the insertion of an aeration stone on the end of the compressed air line, with the stone submerged below the liquid line to offer greater air transfer into the liquid during operation. Due to the unreliability and poor mixing performance of the standard stir bar, the stir bar was replaced with a flat magnetic stir bar (star design). Mixing and aeration

performance visibly improved with these reactor alterations, as evidenced by the appearance of smaller bubbles and a larger vortex at the liquid surface.

Methods

An aqueous ROC20 solution was formulated using a step-wise solution formulation process. The basic approach involved creating an amine solution at 55°C and atmospheric conditions, then sparging CO_2 to load the system. Amine was then added to achieve the final ROC20 formulation. Of note: when the amine solution was loaded with CO_2, a distinguishable liquid-liquid interface was observed which appeared as a layer of liquid (lower) undergoing loading (CO_2) sparging that grew in thickness over time, until nearly reaching the top of the liquid column; the top, more opaque layer decreased in thickness as the loading was implemented. The CO_2 sparging rate was adjusted to prevent the CO_2 bubbles from reaching the surface; the liquid-liquid interface position relative to the top of the liquid column correlated with the rise of CO_2 bubbles in the column.

The ORP of ROC20 solutions was measured following the ASTM Method D1498-07. All equipment including the reference electrode (Ag/AgCl), measurement electrode (platinum), meter, and standard and reference solutions adhered to recommendations in the ASTM Standard. Methodologies also adhered to the ASTM Standard including the use and frequency of equipment reference measurements, the cleaning of the probe and sample measurement approach (collecting successive readings until a change of no more than 10 mV is observed). Temperature was recorded during each experiment to allow for any corrections in ORP measurements needed (none were made). The electrode has been stored in a dilute aqueous solution of Ag/AgCl as recommended by the manufacturer.

Quinhydrone/water reference buffer solutions of pH 4 and 7 were created and utilized each day that ORP measurements were collected on reactor solutions. The standards were used as described in the ASTM standard for checking instrument response prior to use each day. For the pH 4 solution at 25 °C, the ORP reading should be 263 mV +/- 30 mV; actual measurements were typically in the range of 246 to 253 mV at 23 C.

ORP Measurements

We created a ROC20 solution loaded to 0.3 M/M as described above. This solution was loaded in the jacketed reactor with aeration, stirring and heating in the jacket as follows: jacket temperature 55°C, reactor temperature 53.5°C, aeration rate 2.6 ml/s, and stirring bar set at 400 rpm. These operating conditions were maintained for a period of two days. As discussed above, the reactor was shut down and changes were made to provide greater mixing and aeration of solution. After making hardware alterations, the reactor was operated with the ROC20 solution, and ORP measurements were collected, as reported below. Notably, the aeration flow rate was increased for all follow-up experiments with the exception of the quiescent reactor experiment described below.

Due to the relatively poor performance of the initial reactor configuration with respect to oxygen transfer into solution, experiments were limited to two series. The first series included the use of a ROC20 solution (loaded 0.3 m/m), with ORP measurements made to test the viability of the system set-u, and the effect on ORP of copper (cupric

sulfate) in solution, and the second series using ROC20 and improved mass transfer of air/oxygen into solution.

Results

Oxidation-Reduction Potential

The ORP probe function was checked with quinhydrone reference solutions formulated each day that ORP measurements were collected. ORP response for the pH 4 and 7 solutions were typically in the range of 246 to 279 millivolts (mV) and 64 to 79 mV at 23°C, respectively. The ASTM standard recommends that the nominal ORP of the two reference standards be 263 and 76 mV, respectively for the pH 4 and 7 solutions. ORP measurements in the reference solutions were consistent with these values for the entire two months during which periodic measurements of the solution were recorded.

On initial operation of the reactor with a ROC20 solution (0.3 loading) at a typical temperature of 53.5°C (jacket at 55°C), ORP measurements were in the range of -179 to -181; these measurements correspond to operation of the reactor prior to the improvements in aeration and mixing. After the initial measurements were made, sufficient cupric sulfate solution was added to the solution to achieve 0.001 mmolar copper in solution. The ROC20 solution immediately turned a light blue color. Two minutes after adding the copper solution, the ORP was measured at -145 mV. An additional amount of cupric sulfate solution was added to the solution to increase the copper concentration to 0.01 mmolar Cu^{2+}. The solution immediately responded by turning a darker blue, and within one minute of addition of cupric sulfate solution, the ORP was measured at -80 mV.

Following the collection of the initial ORP measurement data described, the reactor was shut down for approximately three weeks. The ROC20 solution (with copper) was left idle in the covered reactor during this period. After modifications were made to the reactor, experiments were resumed. With a sparge stone (Fisher, Diffusion Stone Cylinder) and mixing star magnet, improved dispersion of air in the system was achieved. However, the group observed that the ROC20 solution exhibited a greater viscosity, as evidenced by a greater difficulty in achieving stable rotation of the mixing magnet. The stir bar mixing rate speed was limited to approximately 260 rpm under these conditions. While being mixed, the solution partitioned into two layers of differing shades of blue and levels of opacity, possibly as a result of diminished mixing efficiency due to higher solution viscosity. The viscosity of this solution was measured using a Physica MCR300 instrument. That data is presented below.

A set of experiments was then run on a ROC20 solution created with the remainder of a lower molality solution set aside from the earlier formulation of the initial step-wise formulation of ROC20; this solution was brought up to ROC20 concentration with the addition of sufficient amine at 40°C to achieve the desired concentration. No difficulty was encountered in dissolving the amine to achieve the ROC20 formulation.

Table 1: (caption)

Aeration/ORP Study No. 1					
Time (s)	ORP (mV)	Temp (°C)	Time (s)	ORP (mV)	Temp (°C)
-10	-164	52.5	330	-244	53

0	-167	52.5	360	-249	53
15	-170	52.5	390	-252	53
25	-172	52	420	-255	53
40	-176	52.5	450	-258	53
55	-179	52.5	480	-260	53
60	-180	53	540	-265	53
75	-182	53	600	-267	53
90	-184	53	660	-270	53.5
120	-192	53	720	-271	53.5
135	-197	53	840	-274	53.5
150	-202	53	1100	-279	53.5
165	-208	53	1440	-282	53.5
180	-212	53	1800	-283	53.5
210	-220	53	2280	-285	53.5
225	-224	53	6180	-291	53.5
240	-228	53	8100	-292	53.5
270	-234	53	9900	-292	53.5
285	-236	53	15600	-294	53.5
300	-239	53			

Two series of experiments were run on the reactor to investigate ORP response. The first was designed to investigate ORP changes after achieving well stirred and aerated conditions for over two hours. The reactor stirring and aeration were shut down and measurement of ORP was implemented by leaving the probe in solution and recording ORP and temperature until changes of less than one mV were observed. The reactor jacket water was kept in circulation to maintain a nearly constant temperature of 53.5 to 54°C. The data are tabulated in Table 1 of this report, and plotted in Figure 1 as ORP vs. time. The data indicate that the solution ORP rapidly decreased from an ORP of -164 mV to -250 within six minutes, and reached a point of limited changes in ORP after approximately 25 minutes and an ORP measurement of approximately -285 mV. A final ORP of -294 mV was reached after 4 hours and 20 minutes with the reactor lying quiescent.

A second series of measurements was made utilizing the same reactor and solution configuration and conditions. In this case, the reactor was taken from a quiescent state to being fully aerated and stirred, with ORP measurements made in real time immediately after start-up. As before, the jacket water was kept circulating to maintain the reactor at a nearly constant temperature of 53.5°C. The data from this experiment are tabulated in Table 2 and plotted in Figure 2. .

Table 2: **Aeration/ORP Study No. 2, 53.5C, ROC20**

Time (s)	ORP (mV)	Temp °C	Time (s)	ORP (mV)	Temp °C
15	-281	53.5	180	-192	53.5
34	-267	53.5	195	-191	53.5
36	-260	53.5	210	-190	53.5
43	-250	53.5	240	-190	53.5
50	-240	53.5	270	-189	53.5

70	-224	53.5	300	-188	53.5
80	-217	53.5	360	-188	53.5
90	-213	53.5	480	-188	53.5
105	-207	53.5	600	-187	53.5
120	-202	53.5	900	-185	53
135	-198	53.5	2400	-180	53
150	-195	53.5	3600	-182	53

The data indicate that ORP of solution immediately returned to a higher level, and reached an endpoint (-190 mV) wherein little change in ORP occurred after approximately 3.5 to 4 minutes. The final ORP measurement reached in this experiment was -182 mV one hour after start-up of the aeration and mixing.

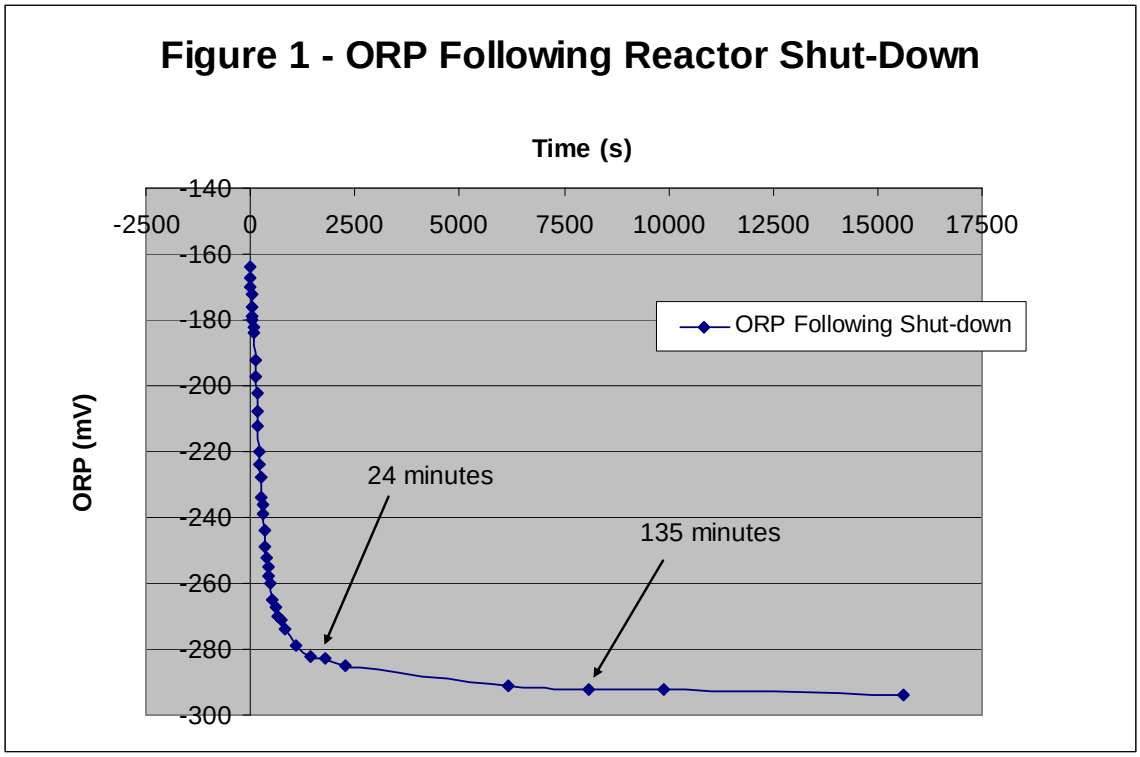

Viscosity

The viscosity of dilute and concentrated ROC20 solutions was measured using a Physica MCR300 viscometer. That data is presented in Table 3 and indicates that the dilute and concentrated ROC20 solutions both exhibited viscosities above that of water, and decreased from 25°C to 40°C as expected. Additionally, the ROC20 solution augmented with 0.01 mmolar Cu^{2+} exhibited a viscosity of approximately 305 cP, which was well above that exhibited by a ROC20 solution without Cu^{2+}. As discussed above, the augmented solution exhibited viscous behavior in the reactor including difficulty of mixing and separation into two layers.

Table 3: (caption)

Viscosity of ROC20 Solutions			
Concentration	CO_2 Loading	Viscosity	Temperature
molality	moles/mole alk	cP	°C
DI Water	0	1	25
dilute	0.3	6.5	25
dilute	0.3	4.5	40
conc	0.3	17.8	25
conc	0.3	10.5	40
conc	0.3	305	25
conc	0.3	110	40

Last two measurements recorded on solution augmented with 0.01 millimolar copper.

The concentrated ROC20 solution with Cu^{2+} exhibiting high viscosity was analyzed using a Dionex LC25 chromatography (cation exchange) instrument along with a ROC20 solution without Cu^{2+} in order to determine whether the higher viscosity in the copper augmented PZ solution could be attributed to the dimerization of amine or an amine breakdown product. That analysis indicated that an additional compound derived from the polymerization of amine did not exist in solution, and that the concentration of amine in each of the ROC20 solutions was similar.

Future Work

The initial work reported here demonstrated that gross measurements of amine solution ORP can be made without drift or degradation in repeatability of results. Sufficient data has not been collected to determine predictive correlations between loading and ORP in solution, or to use ORP measurements as a parameter for measuring oxidation of solvent species and solution degradation in general. Follow-on work will be performed with these objectives in mind. It is currently anticipated that the same reactor configuration will be utilized in future work, until mass transfer limitations prevent the group from obtaining meaningful data.

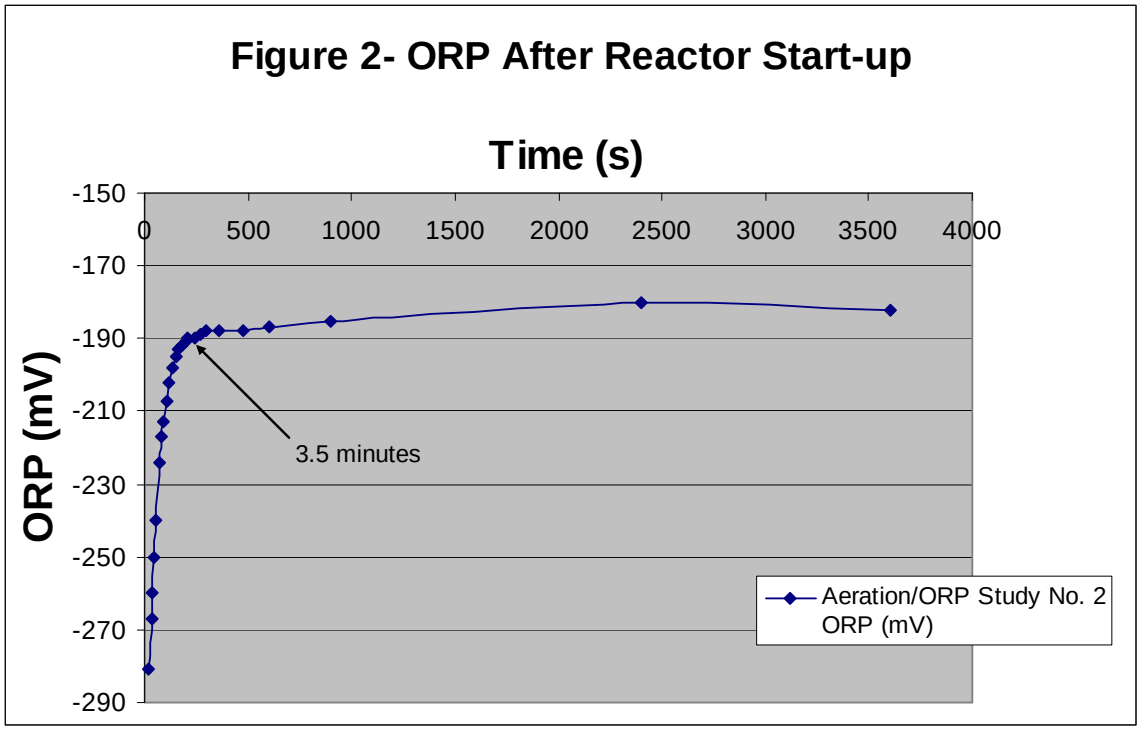

By adding a metal species (copper) to solution in previous experiments, it was anticipated that the ORP of solution would be altered by these metals participating in or catalyzing additional half-reactions. Future experiments with ROC20 will be performed with the addition of ferrous iron at concentrations of 0.01, 0.1, and 1 mmolar to measure ORP changes with this species. Depending on those results, a ferric iron species will be added to solution at similar concentrations to force additional half-reactions to occur and improve understanding of how ORP changes in the presence of iron at various oxidative states. The group will also attempt to describe the chemical interaction of species from an electrochemical standpoint as this work progresses by creating a list of possible half-reactions in the ROC20 solution and their associated potentials. The objectives of this work are to investigate how these metals affect ORP of solution and potentially result in a greater degree of solvent degradation. It is believed that some metals species (cobalt or nickel) serve as catalysts in the breakdown of amine solvents. We will measure ORP in the presence and absence of these species to assess effects on oxidation of solvent.

Our work will attempt to tie ORP activity to degradation of solvent by measuring ORP in reactor over an extended period of time, and with the addition of controlled amounts of metals species. We will analyze solvent solution periodically to confirm the presence and concentration of breakdown products.

Other work to be performed includes further investigation into possible polymerization activity in solution, as evidenced by the ROC20 solution augmented with copper. The group will investigate chelation and polymerization processes for amine solutions in the presence of metals species through a thorough literature review. Solutions exhibiting significant increases in viscosity such as that observed in a ROC20 solution augmented with copper will be tested for the presence of dimers.

Future experiments are anticipated to be maintained at 55°C for up to three weeks to allow for periodic measurements to be made over an extended time and further the group's understanding of degradation of solvent and solvent products over time; the unreliability of reactor operations and need for system modifications prevented the group from achieving this goal in the previous experiments.

One other goal of our work is to determine an upper end to amine concentrations in solution at various temperatures ranging from near-zero to 55°C. Our starting point for implementing this work is the concentration utilized in previous experimental work. We will use formulations of aqueous amine, and add amine to solution at 40 to 55°C, then cool the solution rapidly to observe salting effects at higher concentrations.

A redox standard solution was purchased from Fisher Scientific consisting of an iodide-triiodide solution (Calatogue No. 659532, Ricca Chemical). The standard solution is stable and provides a measurable oxidation-reduction potential; values for an Ag/AgCl probe saturated with KCl at 20, 25, and 30°C are provided in the ASTM Standard as 220, 221, and 222 mV, respectively. This solution will allow us to further standardize the collection of ORP data.

Reclaiming by Crystallization - Potassium Sulfate

3rd Quarter Progress Report 2007

by Qing Xu

Supported by the Luminant Carbon Management Program

Department of Chemical Engineering

University of Texas at Austin

Abstract

One side reaction in CO_2 capture when using MEA/PZ is the generation of sulfate from SO_2. This sulfate has to be removed so that the MEA/PZ solution can be reused for CO_2 capture. Potassium compounds can be used in the removal of sulfate. In order to determine how best to accomplish this, the solubility of potassium sulfate was measured with variable MEA/PZ concentration and CO_2 loading.

In previous work by Xu, solubility measurement was conducted at low temperatures up to 40ºC. A model predicting experimental K_{sp} was developed, with equivalent alkali concentration, temperature, and ionic strength as the variables.

In this report a new method was developed for conducting solubility measurement at high temperatures and high CO_2 loading. The experiment system was well sealed to avoid CO_2 loss under those conditions and got good data.

Based on the previous work of Freguia (2002), new interaction parameters were regressed in this work to match Söhnel's data (1985) in water and the experiment data by Xu. The regression was done using Data Regression System in Aspen Plus®. An interaction parameter set for CO_2-MEA-H_2O-K^+-$SO_4^=$ system in Electrolyte-NRTL model was developed. The model is tested by a series of flash simulations. It can fairly simulate the interactions between ion pairs and molecules within certain condition ranges, but still needs further modification.

Introduction

One side reaction in CO_2 capture when using MEA/PZ is the generation of sulfate from SO_2. This sulfate has to be removed so that the MEA/PZ solution can be reused for CO_2 capture. Potassium compounds can be used in the removal of sulfate. In order to determine how best to accomplish this, the solubility of potassium sulfate was measured with variable MEA/PZ concentration and CO_2 loading.

A new method for conduction of solubility experiments at high temperature

and high CO_2 loading was developed and the results proved to be fair.

Based on previous work of Freguia (2002), several new interaction parameters in Electrolyte-NRTL model for CO_2-MEA-H_2O-K^+-$SO_4^=$ system were regressed using Söhnel's data (1985) in water and the experiment data by Xu and. The regressed result was tested by a series of flash simulations.

Relative saturation, which is representative of the accuracy of the regression result for each experimental data, is dependent on MEA concentration and CO_2 loading, and is independent of temperature. The regression is applicable within a certain range of MEA concentration and CO_2 loading, but still needs modification.

Experiment Methods

CO_2 loading

A bubbler was used to add CO_2 to stock amine solutions (7 m MEA, 11 m MEA, 7 m MEA/2 m PZ, and 4 m PZ). The amounts of CO_2 added into the solutions were weighed by a balance. CO_2 loading is defined as follows:

$$\alpha = \frac{\text{moles of } CO_2}{\text{moles of eq.alkali}}$$

For these experiments, $\text{moles of eq.alkali} = (\text{moles of MEA}) + 2 \cdot (\text{moles of PZ})$

Method 1

50 g of the loaded solution was agitated by a magnetic stir bar through the following process. 0.1-0.4 g K_2SO_4 was sequentially added to the system and conductivity was measured with each addition until the solution was saturated. Then an excess of K_2SO_4 was added to the solution and the final conductivity was recorded. Conductivity was correlated with K_2SO_4 concentration and extrapolated to obtain the K_2SO_4 saturation concentration. The conductivity is temperature dependent.

In modifications of this procedure, KOH or H_2SO_4 was added to the solution before the additions of K_2SO_4. But here KOH is excluded from moles of equivalent alkali for CO_2 loading calculation.

These experiments were conducted at room temperature and 40ºC. A water bath was used to conduct the experiments at 40ºC.

Method 2

This method was used to measure high CO_2 loading solutions at relatively high temperatures.

First, a certain amount of K_2SO_4 was added into a jacketed beaker, and a certain volume (about 40 mL) of the loaded solution was added and weighed. Then the beaker was sealed using a plug with 2 holes, one for a conductivity meter and the other for liquid entrance. The solution was agitated by a magnetic stir bar through the following process. 2.0-3.5 mL loaded solution was sequentially added to the

system through a Brinkmann® bottle top and conductivity was measured with each addition. In the beginning the solution was over saturated with solids, and then got diluted. Conductivity was correlated with K_2SO_4 concentration and extrapolated to obtain the K_2SO_4 saturation concentration.

In modifications of this procedure, KOH or H_2SO_4 was added to the stock solution.

These experiments were conducted at 80ºC. A water bath was used to maintain the temperature.

The experiment apparatus is shown in Figure 1.

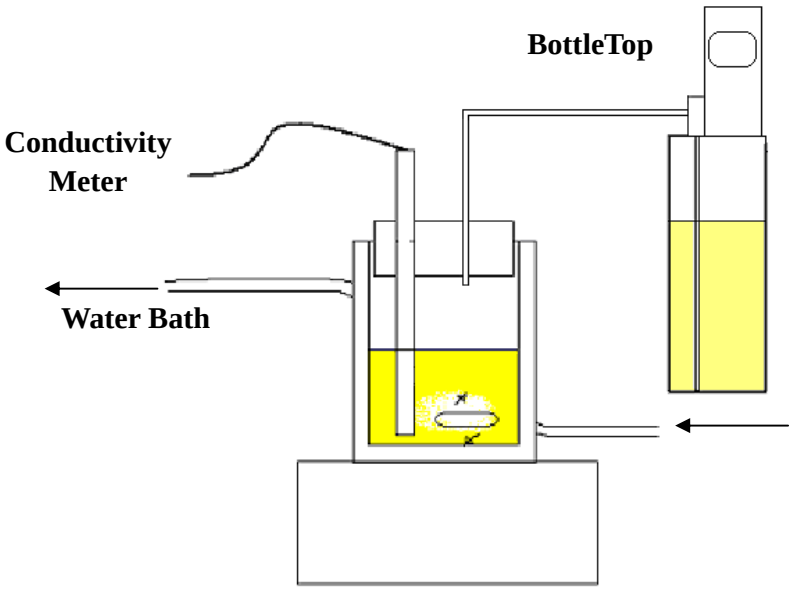

Figure 1: Experiment Apparatus for Method 2

Examples

Following are experimental graph examples. Intersections of the curves are the saturation points, and solubility of K_2SO_4 is calculated from the two equations of the curves. Similar graphs resulted from methods 1 and 2. Method 2 can effectively avoid CO_2 loss, because there is no bend in the curve which represents a composition change of a loaded stock solution.

With an increasing solubility after saturation point:

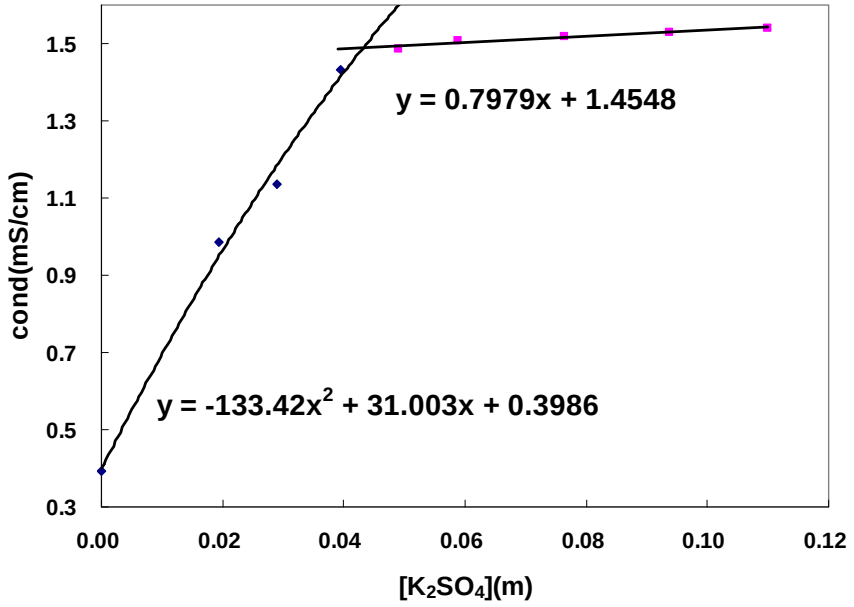

Figure 2: Conductivity dependence on concentration -1
11 m MEA, $[CO_2]_t$=0 m

With a decreasing solubility after saturation point:

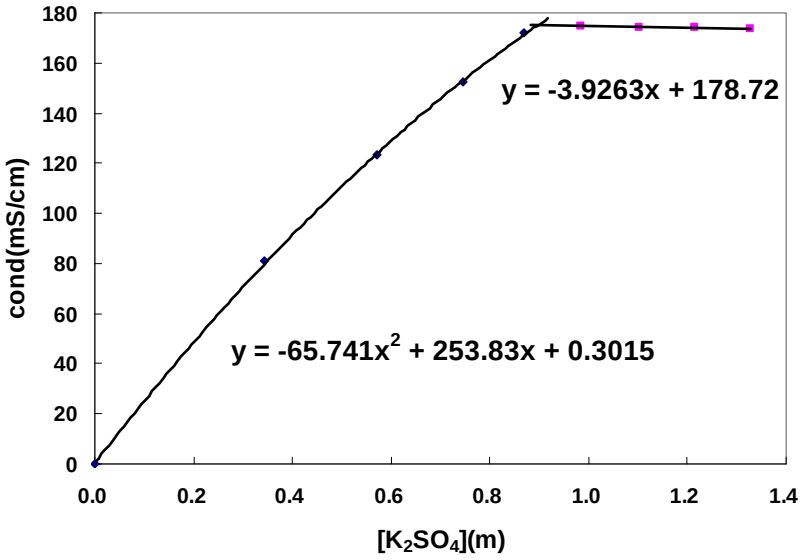

Figure 3: Conductivity dependence on concentration -2
0 m MEA, $[CO_2]_t$=0 m

Data (including previous data)

Table 1: Solubility of K_2SO_4 in amine solution

T(°C)	Concentration(m)					I^a	$Ksp_{exp}{}^b$
	K^+	$SO_4^=$	CO_2	MEA	PZ		
20†	1.268	0.634	0	0	0	1.90	1.020
25†	1.375	0.688	0	0	0	2.06	1.300
30†	1.477	0.738	0	0	0	2.22	1.610
40†	1.700	0.850	0	0	0	2.55	2.456
50†	1.899	0.950	0	0	0	2.85	3.427
60†	2.105	1.053	0	0	0	3.16	4.665
70†	2.301	1.150	0	0	0	3.45	6.091
80†	2.468	1.234	0	0	0	3.70	7.519
23.45	0.614	0.307	2.8	7	0	3.72	0.116
22.25	0.597	0.299	2.8	7	0	3.70	0.107
23.8	0.836	0.218	2.8	7	0	3.46	0.153
24.15	0.205	0.103	0	7	0	0.308	0.004
24.6	0.119	0.060	0	11	0	0.179	0.001
23.95	0.685	0.343	5.5	11	0	5.18	0.161
23.95	0.756	0.378	5.5	11	0	5.28	0.216
22.9	0.766	0.383	5.5	7	2	6.65	0.225
24.1	0.346	0.173	2.2	7	2	2.72	0.021
24.8	0.539	0.270	2	0	4	2.81	0.078
22.85	0.719	0.359	4	0	4	5.08	0.186
40.2	0.887	0.444	5.5	11	0	6.83	0.349
40.1	0.831	0.415	5.5	7	2	6.75	0.287
39.95	0.742	0.371	2.2	3.7	0.8	3.31	0.204
39.9	0.419	0.210	2.2	11	0	2.83	0.037
40	0.618	0.309	1.4	7	0	2.33	0.118
39.95	0.910	0.455	2.8	7	0	4.17	0.377
39.95	0.735	0.193	1.4	7	0	2.15	0.104
40	0.949	0.300	4.4	11	0	0.270	0.270
40	0.594	0.122	2.2	7	2	0.043	0.043
40	0.614	0.457	1.4	7	0	2.62	0.172
39.85	0.678	0.489	4.4	11	0	5.72	0.225
39.9	0.432	0.366	2.2	7	2	3.15	0.068
39.85	0.695	0.173	1.4	7	0	2.09	0.083
39.95	0.435	0.2175	1.88	0	5	2.533	0.041
40	0.7753	0.3876	4.17	0	5	5.331	0.233
24.05	0.086	0.043	0	11	0	0.130	3.229E-04
40.2	0.102	0.051	0	11.4	0	0.154	5.359E-04
22	1.337	0.668	0	0	0	2.005	1.194
45.05	1.796	0.898	0	0	0	2.693	2.895
79.85	1.245	0.622	5.5	11	0	7.367	0.964
79.9	1.351	0.676	2.8	7	0	4.827	1.233
80	1.196	0.423	4.4	11	0	5.843	0.604

T(°C)	Concentration(m)					I[a]	Ksp_{exp}[b]
	K^+	$SO_4^=$	CO_2	MEA	PZ		
79.95	0.992	0.646	4.4	11	0	6.188	0.636
80	0.436	0.218	0	7	0	0.653	0.041
80	0.936	0.618	1.4	7	0	3.105	0.542
41.5	0.925	0.463	2.8	7	0	4.188	0.396

a. I: ionic strength;

b. $Ksp_{exp}=[K^+]^2[SO_4^=]$.

†: from Söhnel, 1985.

Regression Analysis

Theory

The Data Regression System in Aspen Plus® was used to regress for interaction parameters in the Electrolyte-NRTL model from all of the experimental data.

The Electrolyte-NRTL model is originally for aqueous electrolyte systems, and extended to mixed solvent electrolyte systems. It is based on two assumptions: the like-ion repulsion assumption and the local electroneutrality assumption.

τ is the energy parameter, one of the Electrolyte-NRTL parameters, for molecule-molecule, molecule-electrolyte, and electrolyte-electrolyte pairs. It is among the adjustable parameters for the Electrolyte-NRTL model. The values of τ are used in the activity coefficient calculation in the Electrolyte-NRTL activity coefficient model.

For electrolyte-molecule pair parameter, the temperature dependency relations are as follows:

$$\tau_{ca,B} = C_{ca,B} + \frac{D_{ca,B}}{T} + E_{ca,B}[\frac{T^{ref} - T}{T} + \ln\frac{T}{T^{ref}}]$$

$$\tau_{B,ca} = C_{B,ca} + \frac{D_{B,ca}}{T} + E_{B,ca}[\frac{T^{ref} - T}{T} + \ln\frac{T}{T^{ref}}]$$

where

B — solvent molecule

ca — electrolyte pair c and a

$T^{ref} = 298.15K$

GMELCC, GMELCD, and GMELCE are C, D, and E, respectively, but only GMELCC is adjusted in this analysis.

Ksp is the solubility product:

$$Ksp = \prod (x_i \gamma_i)^{\upsilon_i}$$

For K_2SO_4,

$$Ksp = x^2(K^+) \cdot \gamma^2(K^+) \cdot x(SO_4^{2-}) \cdot \gamma(SO_4^{2-})$$

K-SALT is defined as follows:

$$\ln(Ksp) = A + B / T + C * \ln(T)$$

A: K-SALT/1
B: K-SALT/2
C: K-SALT/3
T is in Kelvin.

Regression

K-SALT of K_2SO_4 was regressed from K_2SO_4 solubility data in water (Söhnel, 1985).

The sum of squares of this regression result is 0.313.

Residual root mean square error is 0.250.

Table 2: Regression Result – K-SALT of K_2SO_4

Parameter	Value (SI units)	Standard deviation
K-SALT/1	235.0	2.5
K-SALT/2	-13227	118
K-SALT/3	-36.2	0.4

With these K-SALT values, all the GMELCD were set to be the default value of zero. Existing GMELCC and GMELCD in Aspen Plus® Electrolyte-NRTL model and in Freguia's interaction parameters (2002) were used in this regression. Both experiment data and water data (Söhnel, 1985) were regressed to get GMELCC of all the electrolyte pairs.

GMELCC values were selected that had little correlation with the others. Other parameters were excluded as much as possible to get small standard deviations and small sum of squares.

The sum of squares of this regression result is 10518.

Residual root mean square error is 13.8.

The final regression result is given in Table 3.

Table 3: Regression result – GMELCC

Parameter	Component i	Component j	Value (SI units)	Standard deviation
GMELCC/1	H_2O	$(K^+,MEACOO^-)$	6.8	0.2
GMELCC/1	$(MEA^+,SO_4^=)$	MEA	-4.7	0.5

The other GMELCC parameters were automatically set to be default values as below:

Table 4: Default values of GMELCC

Component i	Component j	Value (SI units)
H_2O	Salt	8
Salt	H_2O	-4
MEA	Salt	15
Salt	MEA	-8

The parameter set of two regressed values and default values was thus developed; this set is expected to simulate the interaction between ion pairs and molecules within certain condition ranges.

Test for regression

The Electrolyte-NRTL model in Aspen Plus®, with the developed GMELCC parameter set above, was input to a series of flash simulations, using each of the experimental conditions, to get the activity coefficients and mole fractions of K^+ and $SO_4^=$, as well as the relative saturation of K_2SO_4. The relative saturation is calculated from the equation below:

$$\text{Relative Saturation} = \frac{\text{Ksp(from fraction and activity coefficient)}}{\text{Ksp(from K - SALT)}}$$

$$= \frac{x^2(K^+)\cdot\gamma^2(K^+)\cdot x(SO_4^{2-})\cdot\gamma(SO_4^{2-})}{\text{Ksp(T)}} = \frac{\alpha^2(K^+)\cdot\alpha(SO_4^{2-})}{\text{Ksp(T)}}$$

Relative saturations of both experiment and water data (Söhnel, 1985) are around 1, which illustrates that the regression is correct.

Discussion

The dependence of relative saturation on temperature, MEA concentration, and CO_2 loading are studied. The prediction of K_{sp} using K-SALT is tested by experiment data.

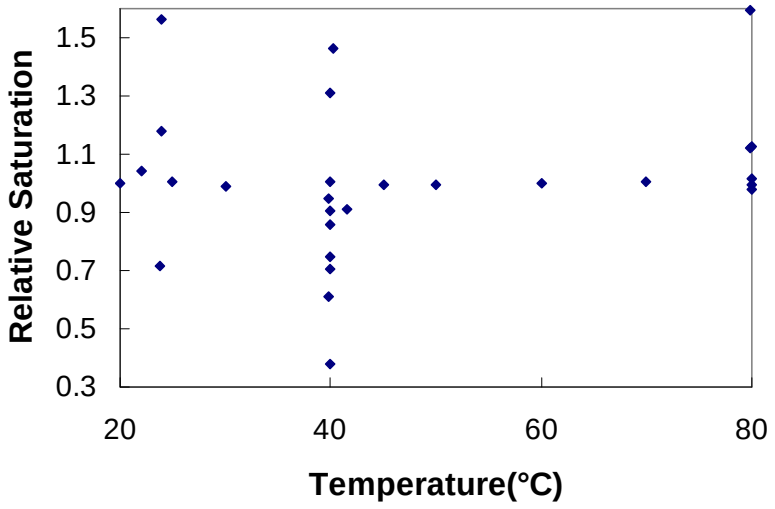

Figure 4: Dependence of Relative Saturation on Temperature

There is no obvious effect of temperature on relative saturation.

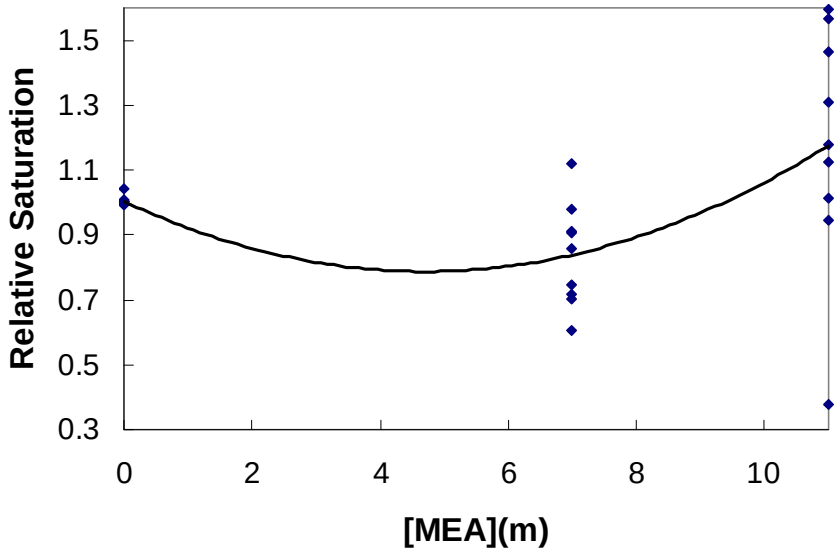

Figure 5: Dependence of Relative Saturation on MEA concentration

At high MEA concentrations, the relative saturation tends to be higher. Data is still needed for 4 m MEA solution to verify this curve. This may be because only two parameters related to MEA are adjusted, while the others are set at default values. They are not good enough to represent the interaction of MEA-related molecules and ions, especially when MEA has high concentration.

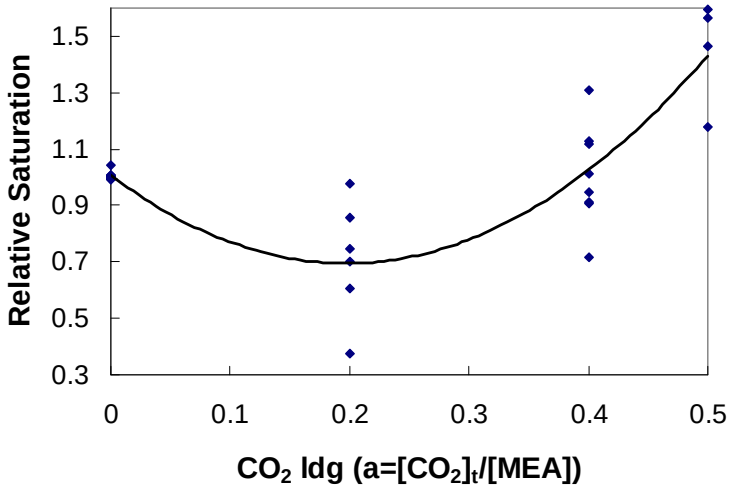

Figure 6: Dependence of Relative Saturation on CO_2 loading

At high CO_2 loading, the relative saturation tends to be higher, but there is a bend at 0.2 of CO_2 loading. This may be because only one parameter related to CO_2 was adjusted, while the others were set at default values.

Figure 7 also illustrates the CO_2 loading effect. Higher loading increases the relative saturation.

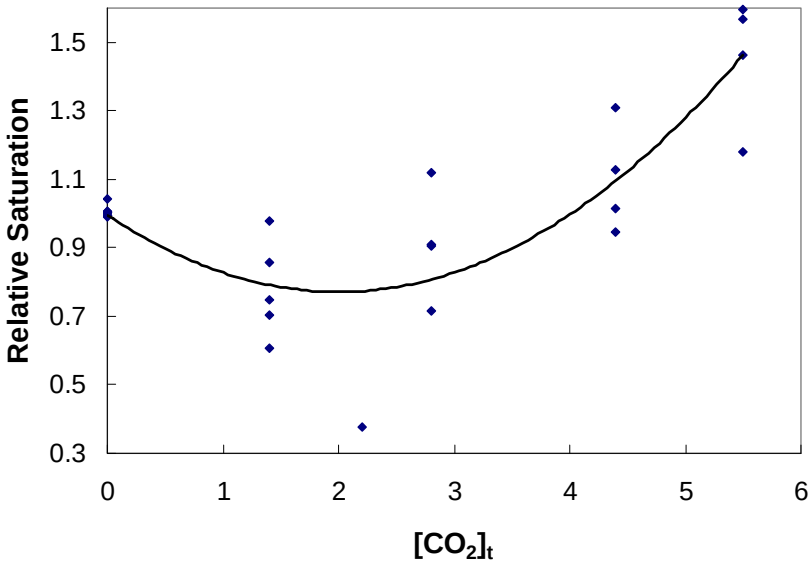

Figure 7: Dependence of Relative Saturation on $[CO_2]_t$

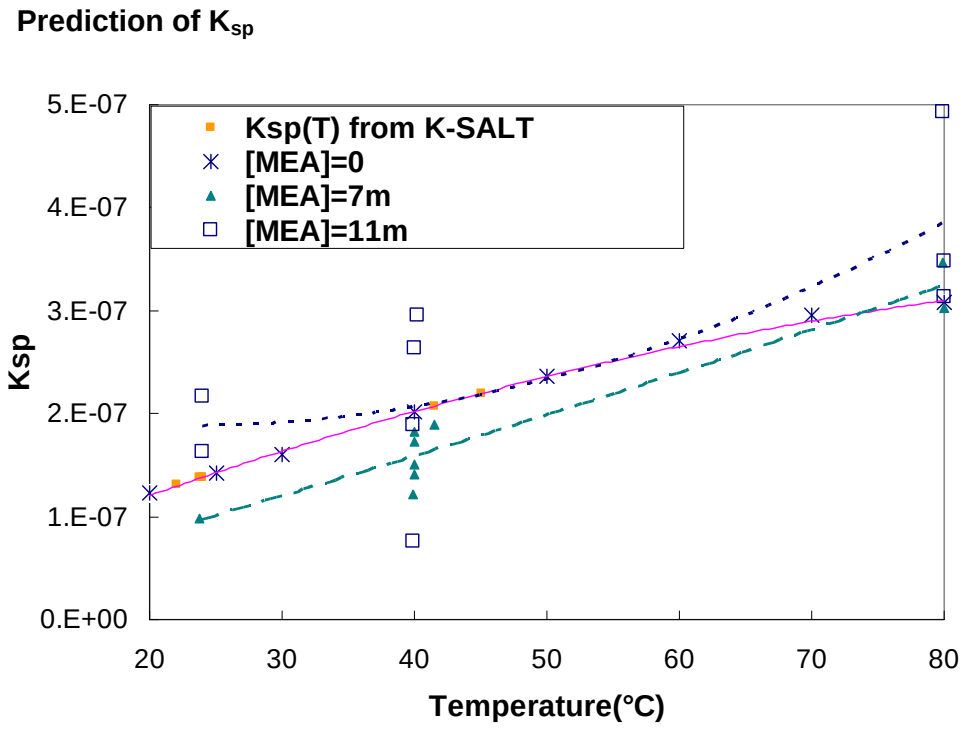

Figure 8: Prediction of K_{sp} using K-SALT

According to Figure 8, when MEA concentration is 0, the data fits the $K_{sp}(T)$ curve well. When MEA concentration is 7 m, some of the experiment data are off the $K_{sp}(T)$ curve because of CO_2 loading. From Figure 6 when CO_2 loading is 0.2 or 0.5, experimental points are away from the $K_{sp}(T)$ model. When MEA concentration

is 11 m, the error becomes bigger, which can also be concluded from Figure 5. Therefore both MEA concentration and CO_2 loading have effects on the prediction of K_{sp} using $K_{sp}(T)$ equation, because the interaction between ion pairs and molecules are different from that inside K_2SO_4-water solution, where the $K_{sp}(T)$ equation is derived from.

Conclusions

One method for conducting solubility measurements at high temperature and high CO_2 loading was developed. This can effectively avoid CO_2 loss.

A new parameter set in Electrolyte-NRTL model for the CO_2-MEA-H_2O-K^+-$SO_4^=$ system was developed. It can fairly simulate the interactions between ion pairs and molecules within certain condition ranges.

Relative saturation, which is representative of the accuracy of the regression result for each experimental data, is dependent on MEA concentration and CO_2 loading, and is independent of temperature. The regression is applicable within a certain range of MEA concentration and CO_2 loading, but still needs modification.

Future work

Modify the regression of MEA experiment data; get a more accurate GMELCC/GMELCD parameter set for the energy parameter τ. Find out the interactions between ion pairs and molecules in CO_2 loaded MEA solution.

Conduct experiments with 3.5 m or 4 m MEA solution.

Conduct experiments using other loaded amine solutions, as PZ, AMP, MDEA, etc.

Measure the rate of CO_2 loss.

Conduct experiments of K_2SO_4 continuous crystallization.

Reference

Freguia, S., "Modeling of CO_2 Removal from Flue Gases Using MEA," M.S. Thesis (2002).

CRC Handbook of Chemistry and Physics, 87th edition, online, section 8-114, http://www.hbcpnetbase.com/articles/08_21_86.pdf

Söhnel, O., and Novotny, P., Densities of Aqueous Solutions of Inorganic Substances, Elsevier, Amsterdam, 1985.

Aspen Plus® help: Electrolyte-NRTL activity coefficient model, etc.

Physical Properties and Mass Transfer Mechanism in Loaded MEA Solution in the Stripper of CO_2 Capture

3rd Quarter Progress Report, 2007

by Sepideh Ziaii Fashami

Supported by the Luminant Carbon Management Program

Department of Chemical Engineering

University of Texas at Austin

Abstract

An accurate dynamic model for a process has to be both rigorous enough to reflect the process complexity and simple enough to ensure the feasibility of process simulations. For simulation of dynamic behavior of the stripper, fundamental understanding of mass and heat transfer in the presence of reactions is required. In addition, the simulator should use proper correlations that predict physical properties and parameters of reactions accurately. Therefore, we have developed correlations for predicting density and viscosity of loaded MEA solution based on available experimental data. We obtained concentration-based equilibrium constants, vapor pressure, heat of absorption, and Henry's Law constant of CO_2 versus temperature, loading, and MEA concentration with E-NRTL framework modified by Hilliard (2007). In addition, the mass transfer mechanism in the presence of equilibrium reactions in the liquid phase is described and formulated.

Introduction

In dynamic analysis and control design of an absorption/stripping CO_2 capture model, the stripper is the most important part of the plant and an accurate dynamic model is a valuable tool to gain insight into complex transient conditions such as start up, shutdown, and load change during an operation. The purpose of this work is to understand the concepts of mass transfer in the presence of reactions between CO_2 and MEA in the stripper. Good insight into the mass and heat transfer mechanisms can help us to make reasonable assumptions that make the mathematical model simple and usable in a dynamic simulator. In this report, concentration-based equilibrium constants of the governing equilibrium reactions, obtained with the most updated Electrolyte-NRTL framework, are given versus temperature, loading, and MEA concentration. Because an accurate estimation of physical properties is an important part of a simulator, correlations, properly predicting viscosity and density of loaded MEA, are included in this report.

Physical properties of loaded MEA solution

Viscosity

Viscosity of loaded MEA solution is correlated using two sets of data. The first set, provided by Weiland et al. (1998), are experimental data that include viscosities of loaded MEA for different loadings and concentration at 25°C. e second data set by Littel et al. (1991) is a correlation for viscosity as a function of concentration and temperature for unloaded MEA. The new correlation for the viscosity of loaded MEA, obtained using the above-mentioned data, is presented below and is a function of concentration of MEA, loading, and temperature.

$$\ln \mu_{MEA} = A(w) + B(w)ldg + C(w) / T \qquad (1)$$

where

$A(w) = \ln(0.0022 * w^2 - 0.0536w + 2.0497) + (0.0006w^2 - 0.1028w - 5.5445)$

$B(w) = 0.0398w - 0.2631$

$C(w) = -0.1788w^2 + 30.6344w + 1652.3$

μ_{MEA} : Viscosity (mPa.sec)

w : MEA concentration (weight %)

ldg : Loading

T : Temperature (K)

The following figures, which plot the viscosity versus temperature, loading, and concentration of MEA solution and are generated by the new correlation, show that the correlation can smoothly predict the viscosity without numerical difficulties.

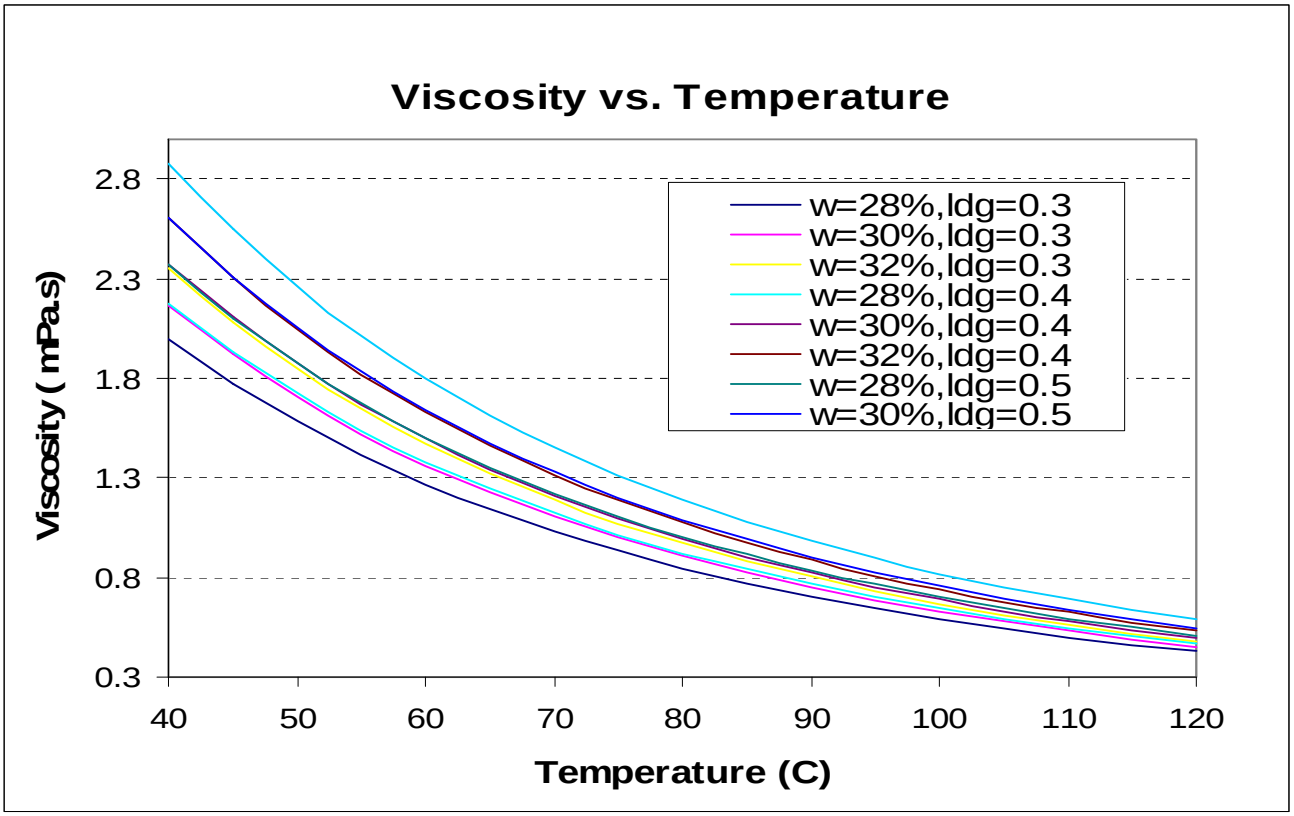

Figure 1: Viscosity of Aqueous MEA

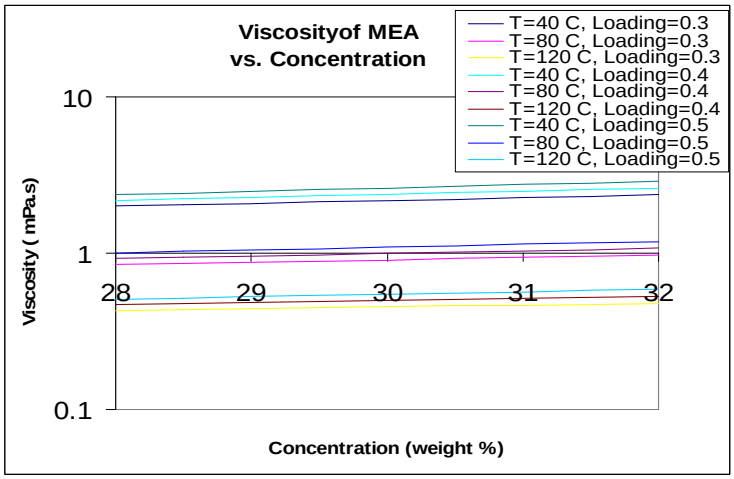

Figure 2:Viscosity of MEA versus concentration at different loadings and temperatures

Density

Density of loaded MEA, like viscosity, is correlated using two sets of data. The first set, provided by Weiland et al. (1998), include densities of loaded MEA for different loadings and concentration at 25^{o}C. The second data set, Littel et al. (1991), is a correlation for density as a function of concentration and temperature for unloaded MEA. The new correlation for the

density of loaded MEA, obtained using above-mentioned data, is presented as follows and is the function of concentration of MEA, loading, and temperature.

$$\rho_{MEA} = -0.4614(T - 298.15) + (6.2842w + 17.425)ldg + 0.484w + 997.9 \quad (2)$$

where

ρ_{MEA} : Density (Kg/m^3)

w : MEA concentration (weight %)

ldg : Loading

T : Temperature (K)

Figures 3 and 4 are plots of density versus temperature, loading, and concentration of MEA solution that are generated by the new correlation, which show that the correlation can smoothly predict the density without numerical difficulties.

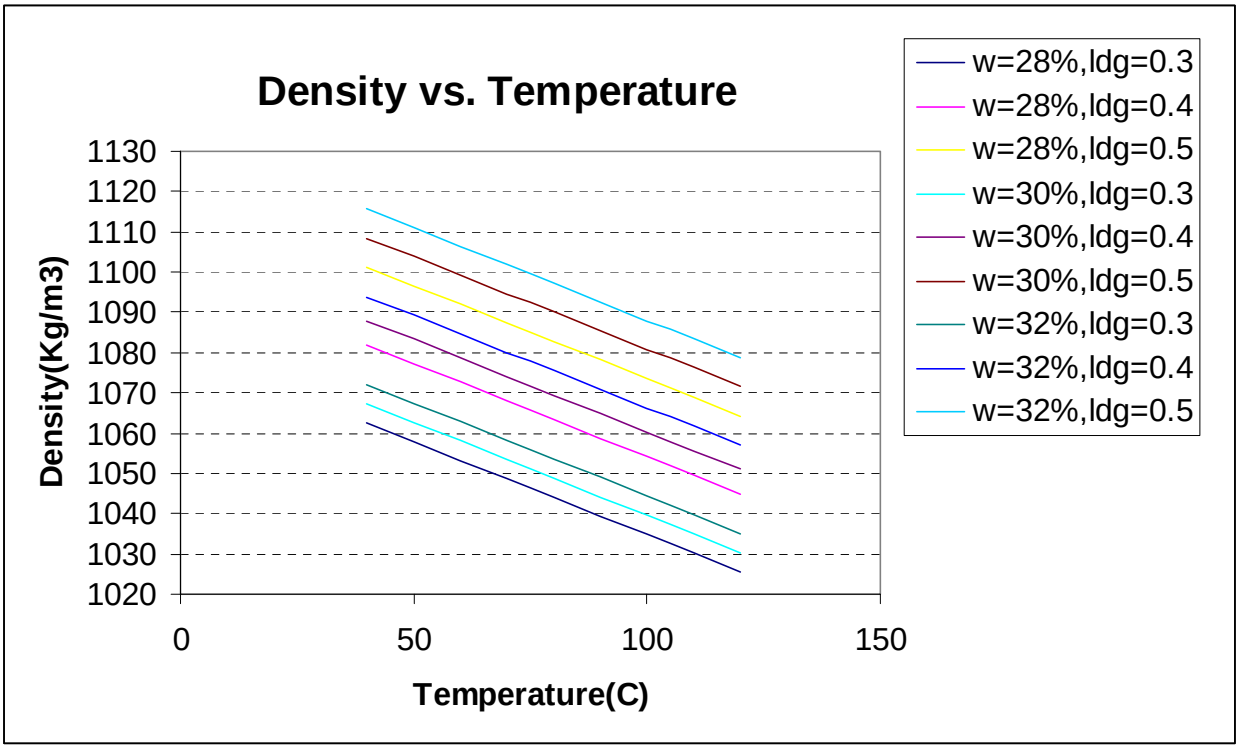

Figure 3: Density of MEA versus temperature at different loadings and concentrations

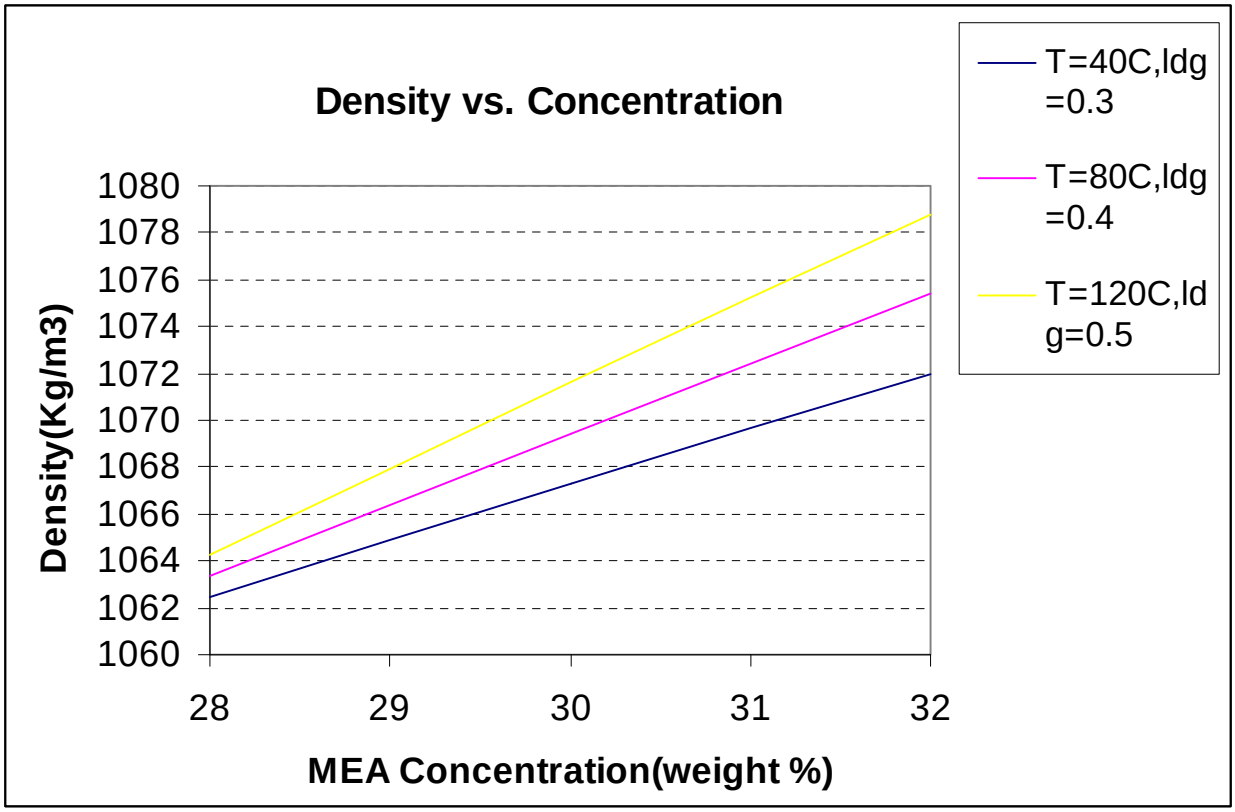

Figure 4: Density of Aqueous MEA loaded with CO_2

Reactions and Equilibrium constants

In the stripper, the reactions involving CO_2 are considered to be at equilibrium due to high operating temperature. The governing reactions in the stripper are carbamate and bicarbonate formation (3), (4):

$$2MEA + CO_2 \overset{K_{carbamate}}{\leftrightarrow} MEACOO^- + MEA^+ \qquad (3)$$

$$MEA + CO_2 \overset{K_{bicarbonate}}{\leftrightarrow} HCO_3^- + MEA^+ \quad (4)$$

The concentration-based equilibrium constant values for these reactions are obtained using modified Electrolyte-NRTL framework, developed by Hilliard (2007), for loaded MEA solution as a function of temperature, loading, and concentration.

Table 1: Equilibrium constants from Hilliard E-NRTL model

Eq. No.	Equilibrium Constant	$\ln(K_{eq}) = a + \frac{b}{T} + c\ln(T) + dT + eldg - fC$					
		a	b	c	d	e	f
3	$K_{eq,carbamate} = \frac{[MEACOO^-][MEA^+]}{P^*_{CO_2}[MEA]^2}$	-1294.4	46361	216.9772	-0.3339	7.2816	-0.3073

4	$K_{eq,bicarbonate} = \frac{[HCO_3^-][MEA^+]}{P^*_{CO_2}[MEA]}$	2727.5	-78283	-465.5435	0.6052	8.1898	-0.3337

where

ldg : Loading

C : MEA concentration (molal)

T : Temperature (K)

$P^*_{CO_2}$: Partial pressure of CO_2 (Pa)

$[HCO_3^-],[MEA^+],[MEA],[MEACOO^-]$: Concentration (molar)

Vapor pressure, Henry's constant and Heat of vaporization of CO_2

The following correlations for vapor pressure, Henry constant, and heat of vaporization of CO_2 are obtained using modified E-NRTL, developed by Hilliard (2007), as a function of temperature, loading, and concentration.

$$\ln(P_{CO_2}(Pa)) = 35.2329 + 16.9227ldg - \frac{9446}{T} + 6961600(\frac{ldg}{T})^2 - 1230100(\frac{ldg}{T^2}) - 12469(\frac{ldg}{T}) + 0.3445C \quad (5)$$

$$\Delta H_{absorption,CO_2}(J/mol) = 8.314(-9446 + 13923200(\frac{ldg^2}{T}) - 2460200(\frac{ldg}{T}) - 12469ldg) \quad (6)$$

$$\ln(H_{CO_2}) = 17.7135 - \frac{957.8597}{T} + 23771(\frac{ldg}{T}) + 194360(\frac{ldg}{T})^2 - 3385500(\frac{ldg}{T^2}) + 37.442ldg + 0.1158C \quad (7)$$

where $H_{CO_2} = \frac{P^*_{CO_2}(Pa)}{[CO_2](mol/lit)}$

Mass transfer in liquid phase

1. Assumptions:Film theory is used for mass transfer modeling and surface renewal theory is approximated by the film theory solution with diffusivity ratios replaced by their square roots.
2. Two equilibrium reactions are involved in CO_2 reaction with aqueous MEA and they are assumed to be instantaneous.
3. There is negligible solvent vaporization. $(N_{MEA} \cong 0)$
4. There is no accumulation of CO_2 at the liquid-gas interface. $(N_{CO_2,gas} \cong N_{TotalCO_2,liquid})$

Known variables: (From overall mass balance around a segment of the stripper)

$C_{totalMEA,b}, C_{totalCO_2,b}$: Total concentration of MEA and CO_2 in the bulk of liquid

Unknown variables:

$C_{MEA,b}, C_{CO_2,b}, C_{MEA^+,b}, C_{carb,b}, C_{bicarb,b}$: Concentration in bulk liquid

$C_{MEA,i}, C_{CO_2,i}, C_{MEA^+,i}, C_{carb,i}, C_{bicarb,i}, P_{CO_2,i}$: Concentration in bulk liquid

Equations:

1. $C_{totalMEA,b} = C_{MEA,b} + C_{MEA^+,b} + C_{carb,b} + C_{bicarb,b}$
2. $C_{totalCO_2,b} = C_{CO_2,b} + C_{carb,b} + C_{bicarb,b}$
3. $N_{CO_2} = k_g(P_{CO_2,g} - P_{CO_2,i}) = k_{l,CO2}(C_{CO2,i} - C_{CO2,b}) + k_{l,carb}(C_{carb,i} - C_{carb,b}) + k_{l,bicarb}\ (C_{bicarb\ ,i} - C_{bicarb\ ,b})$
4. $P_{CO_2,i} = H_{CO_2} \times C_{CO_2,i}$
5. $N_{MEA} = 0 = k_{l,MEA}(C_{MEA,i} - C_{MEA,b}) + k_{l,carb}(C_{carb,i} - C_{carb,b}) + k_{l,MEA^+}(C_{MEA^+,i} - C_{MEA^+,b})$
6. $K_{eq,carbamate} = \dfrac{[MEACOO^-]_b[MEA^+]_b}{P^*_{CO_2,b}[MEA]_b^2}$
7. $K_{eq,carbamate} = \dfrac{[MEACOO^-]_i[MEA^+]_i}{P^*_{CO_2,i}[MEA]_i^2}$
8. $K_{eq,bicarbonate} = \dfrac{[HCO_3^-]_b[MEA^+]_b}{P^*_{CO_2,b}[MEA]_b}$
9. $K_{eq,bicarbonate} = \dfrac{[HCO_3^-]_i[MEA^+]_i}{P^*_{CO_2,i}[MEA]_i}$
10. Charge balance in bulk: $0 = C_{MEA^+,b} - C_{carb,b} - C_{bicarb,b}$
11. Charge balance at interface: $0 = C_{MEA^+,i} - C_{carb,i} - C_{bicarb,i}$

There are 11 unknowns and 11 equations, so this system can be completely solved.

Future Work

In future work, the plan is to understand the heat transfer mechanism, make reasonable assumptions, and build an accurate model of mass and heat transfer in segments of a stripper. In addition, we need to find a generic pressure drop correlation for random and structured packing to be used in the dynamic simulator. This understanding can assist in creating a dynamic model of the stripper in Aspen Custom Modeler (ACM) in order to study startup, shutdown and propose a control strategy for the stripper in transient operations.

References

Weiland R. H., J. C. Dingman, D. Benjamin Cronin, and Gregory J. Browning, “Density and Viscosity of some partially carbonated aqueous Alkanolamine solutions and their blends.” *J. Chem. Eng. Data*. **43**, 378-382(1998).

Little R.J., Greet F. Versteeg, and Wlm P.MP. San Swaaij, “Solubility and Diffusivity Data for the absorption of COS, CO_2, and N_2O in Amine solutions.” *J. Chem. Eng. Data*. **37**, 49-55(1992).

Hilliard M., “A Predictive Model for Aqueous Potassium Carbonate/Piperazine/Ethanolamine for Carbon Dioxide Removal from Flue Gas.” Ph.D. dissertation draft, University of Texas at Austin (2007).